

DOE Award No.: DE-FE LBNL-ESD12-001

**Final Report**  
**Properties of Sediments containing**  
**Methane hydrate, water, and gas**  
**Subjected to Changing Gas**  
**Compositions**

Project Period (June 2012 – September 2018)

Submitted by:  
**Tim Kneafsey**



Lawrence Berkeley National Laboratory  
DUNS #:078576738  
1 Cyclotron Road  
Berkeley, CA 94720  
Email: [tjkneafsey@lbl.gov](mailto:tjkneafsey@lbl.gov)  
Phone number: (510) 486-4414

Prepared for:  
United States Department of Energy  
National Energy Technology Laboratory

March 22, 2019



U.S. DEPARTMENT OF  
**ENERGY**

NATIONAL ENERGY  
TECHNOLOGY LABORATORY

Office of Fossil Energy

## **DISCLAIMER**

“This report was prepared as an account of work sponsored by an agency of the United States Government. Neither the United States Government nor any agency thereof, nor any of their employees, makes any warranty, express or implied, or assumes any legal liability or responsibility for the accuracy, completeness, or usefulness of any information, apparatus, product, or process disclosed, or represents that its use would not infringe privately owned rights. Reference herein to any specific commercial product, process, or service by trade name, trademark, manufacturer, or otherwise does not necessarily constitute or imply its endorsement, recommendation, or favoring by the United States Government or any agency thereof. The views and opinions of authors expressed herein do not necessarily state or reflect those of the United States Government or any agency thereof.”

**LBL-ESD12-001**

**Properties of Sediments containing Methane hydrate, water, and gas Subjected  
to Changing Gas Compositions**

**Tim Kneafsey, Sharon Borglin, Seiji Nakagawa**

## Table of Contents

<b>Project Objectives</b> .....	<b>4</b>
<b>Project Description and Report Organization</b> .....	<b>4</b>
<b>1.0 Theme 1. Hydrate-bearing medium property changes due to gas exchange</b> .....	<b>6</b>
1.1 Summary, Interpretation, and Conclusions .....	8
<b>2.0 Theme 2. Computational rock mechanics</b> .....	<b>9</b>
2.1 Summary .....	11
<b>3.0 Theme 3. Layered systems</b> .....	<b>12</b>
3.1 Seven-layer system .....	14
3.1.1 Seven-Layer Test Conclusions .....	17
3.2 Technique development for sand/mud layered systems .....	17
3.3 Summary, Interpretation, and Conclusions .....	18
<b>4.0 Theme 4. Vessel modification</b> .....	<b>20</b>
4.1 New X-ray transparent vessel.....	20
4.2 Summary .....	21
<b>5.0 Theme 5. Thermal Gradients/Chemical Gradients/Well Analogs</b> .....	<b>23</b>
5.1 Impact of a chemical gradient .....	23
5.2 Impact of a Temperature Gradient.....	26
5.3 Impact of Pressure Gradients - Horizontal/Vertical Well Analogs .....	28
5.4 Summary, Interpretation, and Conclusions.....	30
5.4.1. Chemical Gradients .....	30
5.4.2 Temperature Gradients.....	30
5.4.3 Pressure Gradients.....	31
<b>6.0 Other Activities</b> .....	<b>32</b>
<b>References</b> .....	<b>33</b>
<b>Hydrate Papers/Presentations from LBNL Lab</b> .....	<b>34</b>
<b>Appendix A - Experimental Observations of Methane Hydrate Dissociation in Layered Media</b> .....	<b>35</b>

## **LBNL-ESD12-001**

### **Properties of Sediments containing Methane hydrate, water, and gas Subjected to Changing Gas Compositions**

**Tim Kneafsey, Sharon Borglin, Seiji Nakagawa**

#### **Project Objectives**

The overall objective of LBNL gas hydrate laboratory work is to answer questions on the behavior of methane hydrate under natural and engineered conditions and its effects on the media it is in. We strive to support conceptual and numerical model development and parameter estimation. Over the duration of this project, we have focused on gas production from methane hydrate, rather than hydrate-bearing reservoir formation which is another research topic often studied. We use standard laboratory methods, but in addition, have had success using X-ray Computed Tomography to understand process and their spatial distribution.

#### **Project Description and Report Organization**

This project initiated in June 2012 and was completed in September 2018. The project consisted of the following tasks.

- Task 1. Project Management Plan
- Task 2. Measurement of kinetics of gas exchange in hydrate
- Task 3. Investigation of mechanical and hydrologic property changes of methane hydrate-bearing media subjected to nitrogen and CO<sub>2</sub> flushing
- Task 4. Project Management Plan
- Task 5. Measurement of kinetics of gas exchange in a hydrate/water/gas system
- Task 6. Investigation of mechanical and hydrologic property changes of media containing methane hydrate, water, and gas subjected to nitrogen and CO<sub>2</sub> flushing
- Task 7. Grain-scale Computation of Hydrate-Bearing Sand Properties Based on microCT Sample Description (collaboration with NETL)
- Task 8. Gas production from layered hydrate
- Task 9. Comparison of dissociation in hot and cold hydrate (not funded)
- Task 10. Vessel design and Modification
- Task 11. Assessment of thermal gradient modification methods and Investigation of the effect of thermal gradient and gradient oscillation on hydrate behavior
- Task 12. Investigation of the hydrate dissociation point in saline systems with respect to gas production rate
- Task 13. Continued Studies of Hydrate-Bearing Layered Systems
- Task 14. Continued Computational Rock Mechanics
- Task 15. Experimental work in response to current challenges
- Task 16. Continued investigation of layered systems
- Task 17. Comparison of the effect of vertical and horizontal wells for gas production in a layered hydrate-bearing system

For the purposes of this report, we have reorganized 14 tasks into themes that fit together and follow sequentially. Tasks 1, 4, are management tasks and Task 9 was not funded. These three tasks are not discussed below.

**Theme 1. Hydrate-bearing medium property changes due to gas exchange**

Task 2. Measurement of kinetics of gas exchange in hydrate

Task 3. Investigation of mechanical and hydrologic property changes of methane hydrate-bearing media subjected to nitrogen and CO<sub>2</sub> flushing

Task 5. Measurement of kinetics of gas exchange in a hydrate/water/gas system

Task 6. Investigation of mechanical and hydrologic property changes of media containing methane hydrate, water, and gas subjected to nitrogen and CO<sub>2</sub> flushing

**Theme 2. Computational rock mechanics**

Task 7. Grain-scale Computation of Hydrate-Bearing Sand Properties Based on microCT Sample Description (collaboration with NETL)

Task 14. Continued Computational Rock Mechanics

**Theme 3. Layered systems**

Task 8. Gas production from layered hydrate

Task 13. Continued Studies of Hydrate-Bearing Layered Systems

Task 16. Continued investigation of layered systems

**Theme 4. Vessel modification**

Task 10. Vessel design and Modification

**Theme 5. Thermal Gradients/Chemical Gradients/Well Analogs**

Task 11. Assessment of thermal gradient modification methods and Investigation of the effect of thermal gradient and gradient oscillation on hydrate behavior

Task 12. Investigation of the hydrate dissociation point in saline systems with respect to gas production rate

Task 15. Experimental work in response to current challenges

Task 17. Comparison of the effect of vertical and horizontal wells for gas production in a layered hydrate-bearing system

Each theme will be addressed below in sections of the report.

## 1.0 Theme 1. Hydrate-bearing medium property changes due to gas exchange

**Theme Objective:** The objective of this theme was to understand mechanical and hydrologic property changes of methane hydrate-bearing media subjected to nitrogen and CO<sub>2</sub> flushing (23% carbon dioxide -77% nitrogen gas under conditions similar to the ConocoPhillips 2012 Ignik Sikumi Gas Hydrate Field Trial).

A topical report was submitted to NETL on this theme entitled *Properties of Hydrate-Bearing Sediments Subjected to Changing Gas Compositions*. A summary is presented below.

In this theme, we performed a series of carefully controlled laboratory tests in which we monitored changes in methane hydrate-bearing samples when a nitrogen/carbon dioxide gas mixture is flowed through the samples. This was done to provide additional background information related to the Ignik Sikumi field test. In that field test, the same mixture of carbon dioxide and nitrogen was injected into a methane hydrate-bearing unit beneath the north slope of the Brooks Range (North Slope) in northern Alaska (ConocoPhillips 2012 Ignik Sikumi gas hydrate field trial).

Numerous tests were performed. In one series of 17 tests, we measured the kinetic gas exchange rate for different hydrate saturations and different test configurations to provide an estimate for comparison to numerical models. We set our tests up like a gas chromatograph (Figure 1), in which the “column” was the methane hydrate-bearing sand sample akin to the hydrate beneath the North Slope. Methane hydrate was formed using the excess gas technique to distribute it throughout the sand. Following that, the exchange gas (23% carbon dioxide -77% nitrogen) was introduced and flowed at a constant slow rate. Samples were extracted from the effluent and analyzed by direct injection into a gas chromatograph.

In our tests, the exchange rate decreased over the course of time during the tests as methane was depleted from the hydrate. Following the passing of the methane front, the exchange rate ranged from  $3.8 \times 10^{-7}$  moles methane/(mole water\*s) to  $5 \times 10^{-8}$  moles methane/(mole water\*s). In these rates, “moles of water” refers to water originally held in the hydrate to provide a normalizing datum. The reason for the rate decline is likely to be that gas exchange is expected to initially likely occur on the outer surface of the hydrate in a hydrate-bearing medium subject to gas exchange. This hydrate is modified from the injected gas, while not perfectly transformed because the gas composition must change from the addition of methane to the N<sub>2</sub>/CO<sub>2</sub> stream, presents a barrier to gas exchange to the hydrate below the skin. The hydrate then would have a composition gradient from the skin to depth depending on distance from the surface, presence of cracks initially present and caused by structural changes in the hydrate, and guest molecule exchange rate in the hydrate. We would expect that this could be modeled as a diffusive process.

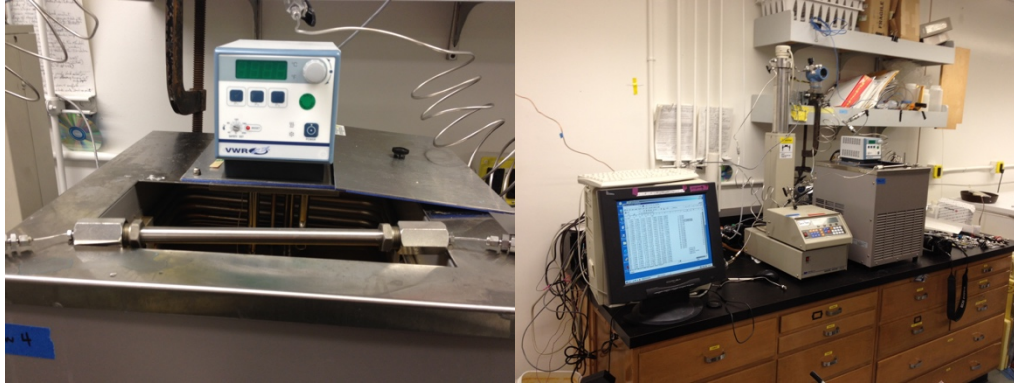


Figure 1. reactor vessel (left) and experiment setup for kinetic measurements.

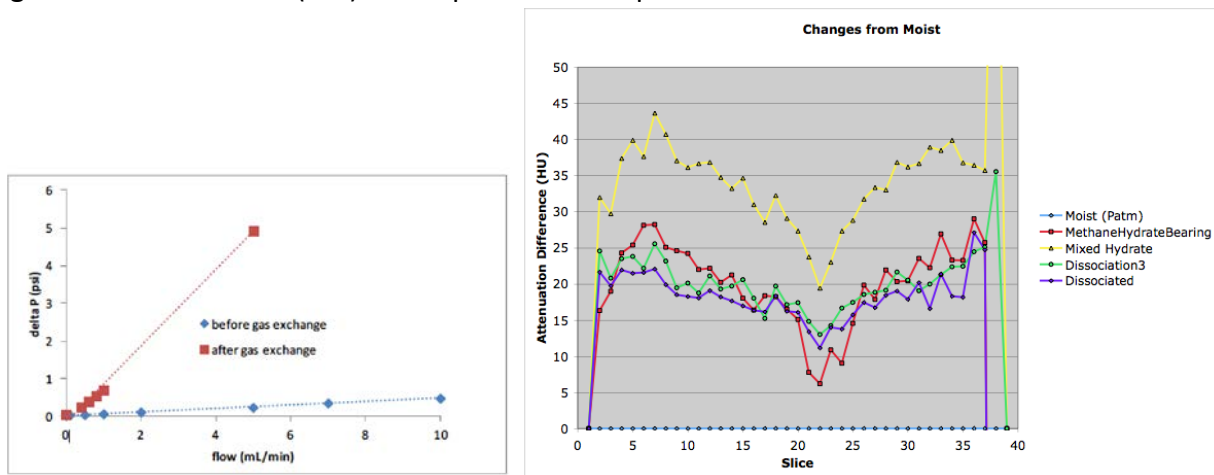


Figure 2. Left - differential pressures across the column indicating a decrease in permeability (higher differential pressure) after gas exchange. Right - X-ray T attenuations along a sample over a variety of conditions including moist sand - blue (the datum), methane hydrate-bearing - red, after mixed hydrate formed - yellow, during dissociation - green, and after dissociation - purple.

In the tests, we monitored permeability, or permeability proxy (differential pressure - Figure 2) to detect hydrological changes caused by gas exchange. We observed no clear trend as permeability increased and decreased as the gas exchange occurred in different cases. This is consistent with other work we have done also supported by NETL (Kneafsey et al., 2010).

In a multi-physics test we used our Split Hopkinson Resonant Bar apparatus (Figure 3) to monitor acoustic resonance of the sample, monitored pressure and temperature, and imaged the sample using X-ray CT scanning. In this test we observed changes in the physical strength of the hydrate-bearing sand during exposure to the mixed gas. ***Upon introduction of the mixed gas, the sample became less stiff and acoustic wave attenuation increased, indicating the presence of liquid water between mineral grains and hydrate. This behavior had not been expected based on hypotheses and lab observations of others. Slow dissociation of the hydrate showed a wide range of hydrate stability conditions as the gas composition changed from dissociation and dilution of the previously injected nitrogen. As mentioned above, the hydrate composition likely had a gradient in composition as well and easily adapted itself to the imposed conditions.***

In the multi-physics test, CT scans showed nonuniform hydrate formation (Figure 2, right), however the relative magnitudes make sense. The blue line (value = 0) shows the starting condition subtracting the starting condition. The formation of methane hydrate caused an attenuation increase as methane mass was added to the structure (e.g. the red line in Figure 2 right), and the mixed hydrate increased the density even more as carbon dioxide and nitrogen (yellow) were included in the gas phase and the hydrate phase.

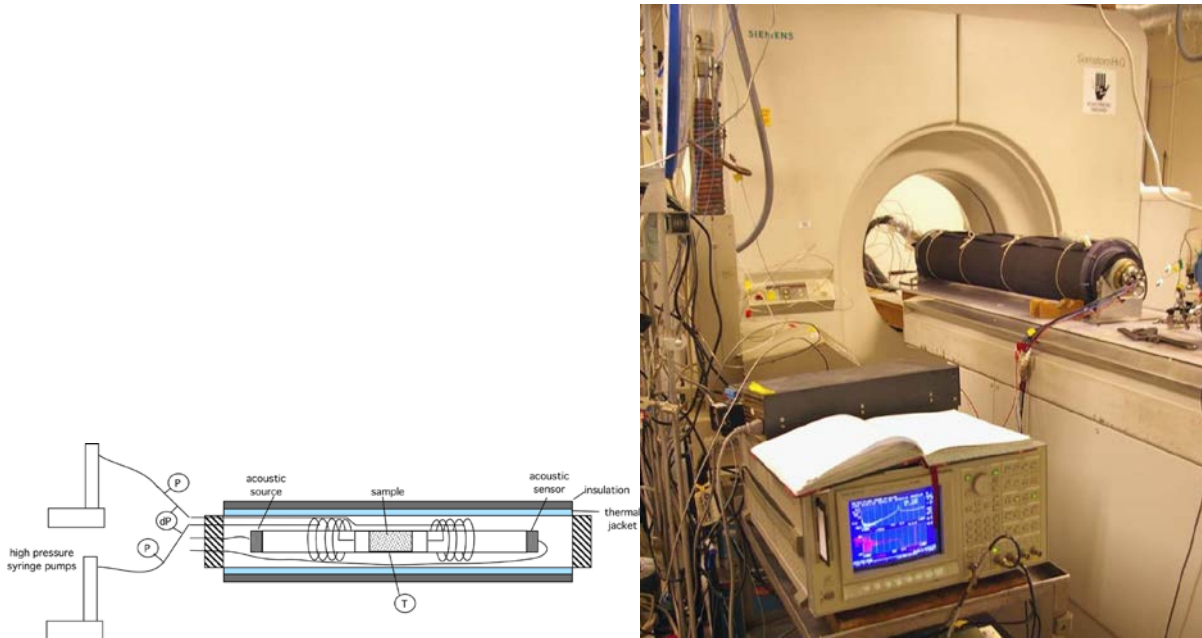


Figure 3. Left – Schematic of the Split Hopkinson Resonant Bar Apparatus showing sample location and appended bars. Right – Pressure vessel with Split Hopkinson Resonant Bar Apparatus setup on the CT table.

### 1.1 Summary, Interpretation, and Conclusions

Injection of mixed CO<sub>2</sub> and nitrogen into methane hydrate-bearing media led to a number of expected and unexpected occurrences. Most importantly, a change in the seismic velocity and attenuation was observed, indicating a softening of the mechanical properties of the hydrate-bearing sediment. In the test performed, the softening was not permanent as the sample stiffened following the initial softening. Changes in permeability were also observed, however the changes were inconsistent in some cases increasing and some cases decreasing. Increasing permeability could occur if hydrate becomes concentrated within certain location and depleted in others in the medium. Decreasing permeability could occur if hydrate volume increased while remaining in the same location or concentrating across the total flow path. Gas chemistry measurements on the outflowed gas indicated a very wide range of conditions similar to a solid solution where a hydrate phase was stable. This resulted in a very long dissociation time as the composition of the hydrate changed responding to imposed conditions. This must be considered in approaching the use of such a technique.

## 2.0 Theme 2. Computational rock mechanics

**Theme objective:** The objective of this work was to evaluate the mechanical impact of different hydrate pore occupancy habits using realistic starting microstructures, consistent 3D image processing, and accurate 3D FEM models to compute key material properties, mainly bulk and shear moduli.

In this theme, we made significant progress on several components including acquisition of a 3D microCT dataset of an Ottawa 20/30 sand sample (mean size  $\sim 600$  microns, however the geometry is more important as the *size can be scaled*) which provided an excellent porous frame for future computational studies. We detailed a sequence of image processing approaches for generating a range of different hydrate cementation styles for elastic property calculation, spanning classical contact, coating, and pore-filling models described by contact cement theory (CCT).

In this theme, we pushed forward calculation of elastic properties using the hydrate pore occupancy models. We developed a MATLAB interface to allow effective utilization of Garboczi's ELAS3D 3D finite-element code in an automated context. The interface performs automatic recompilation of the original F77 code to allow variations in problem size and property as well as automatic calculations on large model suites. The interface has been validated on example problems included in the original code documentation (e.g. spherical inclusions) and tested for scaling out to problems on the order of  $250^3$  voxels ( $15 \times 10^6$  unknowns).

Three hydrate pore occupancy habits were investigated:

- Pore Filling - Nucleation starts in the center of the largest pores and the hydrate grows homogeneously from those nuclei, progressively filling the pore space starting from the bigger pores.
- Cementing - Nucleation starts at grain contacts, and hydrate growth proceeds from the contacts of the grains outwards. This will result in pendular ring-shaped hydrate deposition between the grains, with subsequent coalescence while growing further.
- Surface Coating - Nucleation starts on all the grain surfaces, then grows homogeneously towards the pore space: this provides a uniform coating of the sand grains with hydrate.

These three hydrate growth habits have been used to develop a simple computational protocol capable of providing a theoretical distribution of hydrates in an experimentally measured granular matrix, in this case a quartz sand pack (Ottawa 20/30 was used, as mentioned scale here is selectable) imaged at the Synchrotron X-ray (SXR) microtomography beamline 8.3.2 at the Advanced Light Source (LBNL). The advantage of scanning rather large 600 micron grains is that the grain space and pore space are well-described. Three slices in Figure 4 show the measured sand pack (gray), pore space ( $\sim$ black), and the calculated hydrates distribution (cyan).

The slices in Figure 4 show the calculated volumes in 2D, for clarity, but the model provides 3D data appropriate for pore-scale modeling, and additional phenomenological features can be added. For example, in the three volume renderings presented in Figure 5, we have added a

“temperature gradient” with the bottom of the sample colder than the top, therefore the presence of the hydrate is more pronounced at the bottom of the sample.

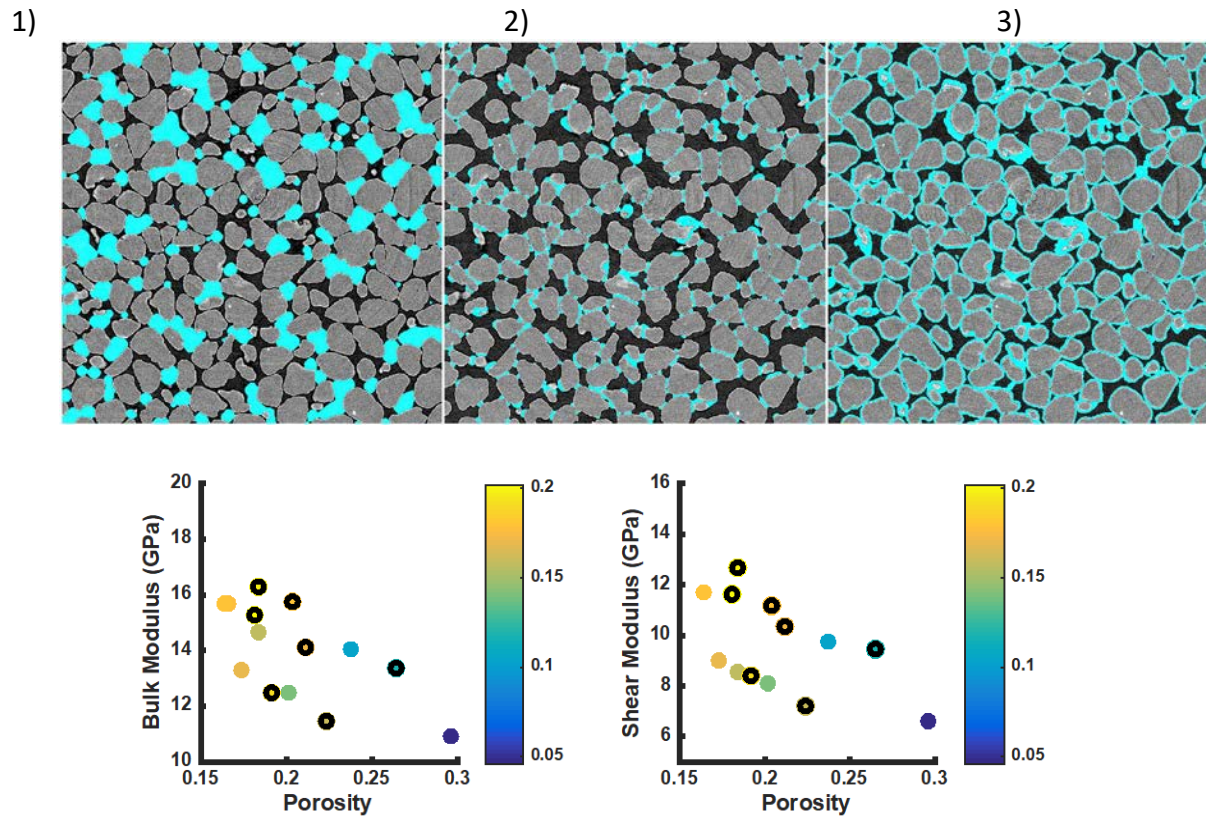


Figure 4 Top: 2D slices from microCT slices of a quartz sand pack with synthetic hydrate distributions showing pore-filling (1), contact cement (2), and grain coating (3) motifs. Bottom: Computed bulk and shear moduli for the grain coating hydrate habit.

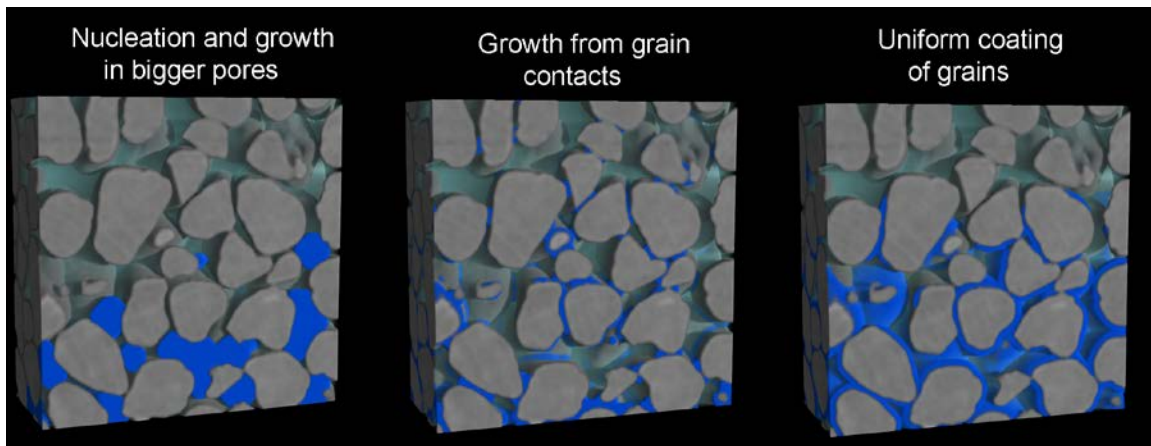


Figure 5 : Volume renderings showing sand grains in grey, water/brine in semi-transparent light blue, and the modeled hydrate in dark blue. Each panel shows a different hydrate habit similar to Figure 4, with the addition of a spatial gradient.

In Figure 5 we show the sand grains in grey, the water/brine in semi-transparent light blue, and the modeled hydrate in dark blue. The colder temperature is at the bottom. The hydrate distribution code starts with the porous matrix and then uses geometric operations based on seed locations determined by the habit type e.g. centroid of the segmented pore (pore filling), grain surface, or contact locations determined by distance maps.

The protocols developed for modeling the theoretical distribution of gas hydrates using the three main concepts in real, measured, sand 3D volumes are completed and, from the figures above, work as expected. At present, the volume generation component of the project is completed and ready for incorporation into the pore-scale modeling tool chain.

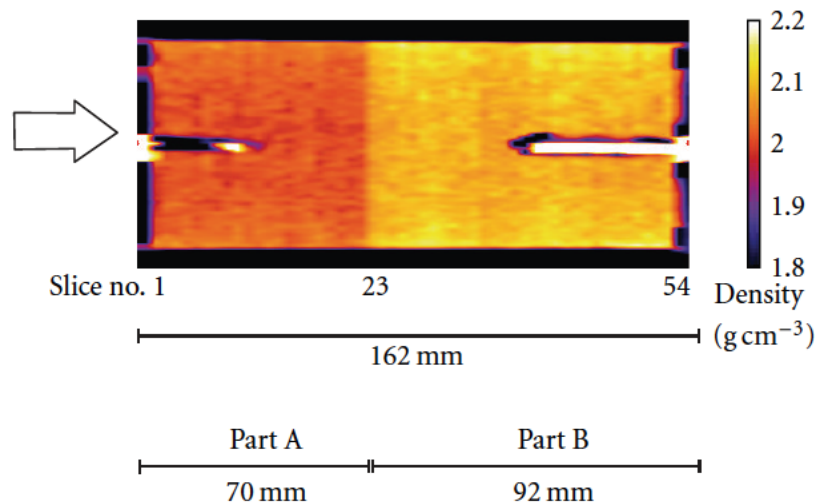
## 2.1 Summary

Three attributes have been targeted for modeling at present, including permeability, diffusivity/formation factor, and elastic properties. The permeability and diffusivity calculation codes were tested and are considered ready for use elsewhere. The permeability code is based on a FD Stokes simulation while the diffusivity code uses a random-walk solver. The third code set, targeting elastic properties, is a finite element solver which requires additional testing.

### 3.0 Theme 3. Layered systems

**Theme objectives:** The nature of a porous medium affects gas and water transport, hydrate formation, gas and hydrate distribution, pressure diffusion, and hydrate dissociation. Even in uniform sands, layers of varying pore sizes exist. Our goal is to understand how these varying pore sizes affect the behavior of hydrate-bearing systems.

Natural systems are heterogeneous and anisotropic. The variations in properties resulting from these heterogeneities and anisotropies will affect the chemical potential distribution and thus the saturation distribution of all the phases including hydrate. An observation of this is shown in Figure 6. In this test, a sandstone sample from the Mount Elbert Stratigraphic Test Well was maintained under equilibrium conditions for nearly 60 days and periodically CT scanned. Even though under equilibrium conditions, gradients were present in the sample including a slight temperature gradient and natural pore size gradients. The result is that the hydrate migrated as a result of these gradients, and hydrate in the subsurface would be expected to do the same thing.



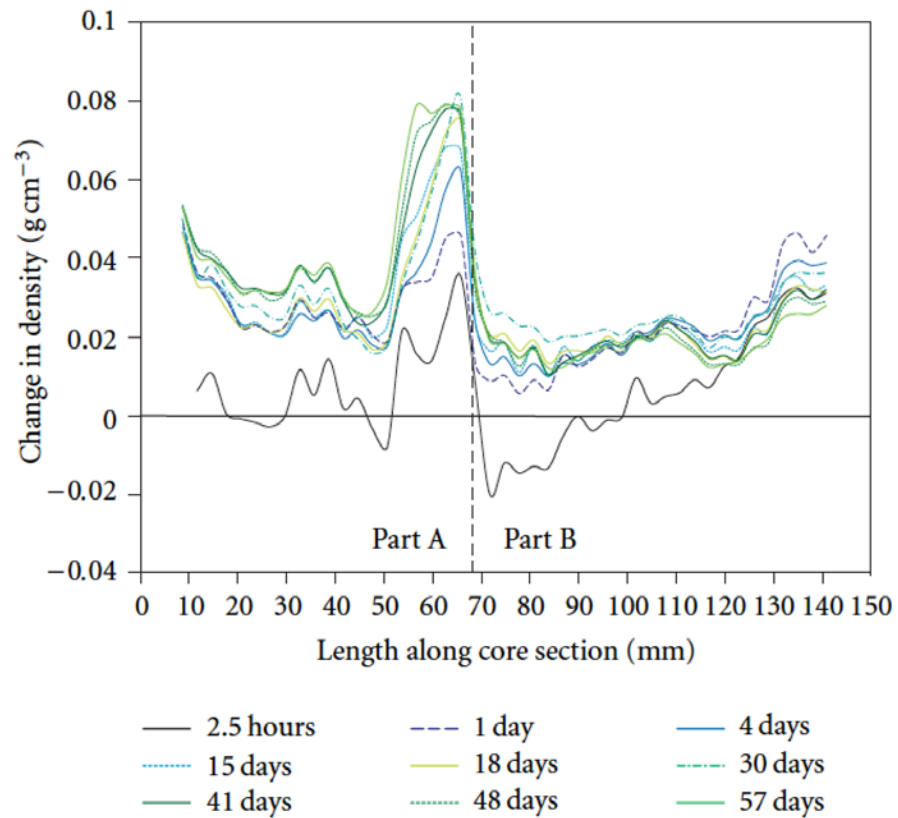


Figure 6. Top – Core density, darker colors represent lower density. The calculated porosities of Parts A and B based on CT images are 0.29 and 0.28, respectively. Part A has a larger average grain size than Part B. Bottom - Density changes over time indicating hydrate migration thought to result from a pore size gradient (Rees et al., 2011).

In an another early laboratory test, researchers set up a complicated multilayered system to investigate the effect of layers under a variety orientations under the same physical conditions (Seol and Kneafsey, 2009, Seol and Kneafsey, 2008) (Figure 7). Hydrate formed, and was strongly affected by capillary pressure gradients affected by the layering, but most strongly affected by the formation of the hydrate itself. Hydrate formation more dramatically affected the gradient than the applied layering in this test as the hydrate changes the capillary pressure when it forms, and exerts cryosuction (Davis, 2001).

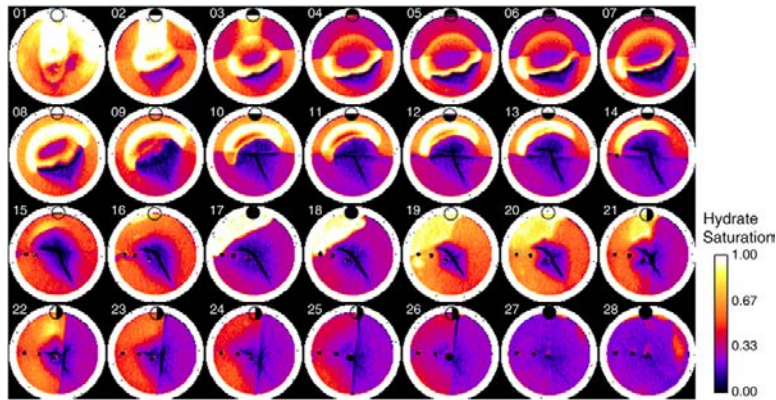
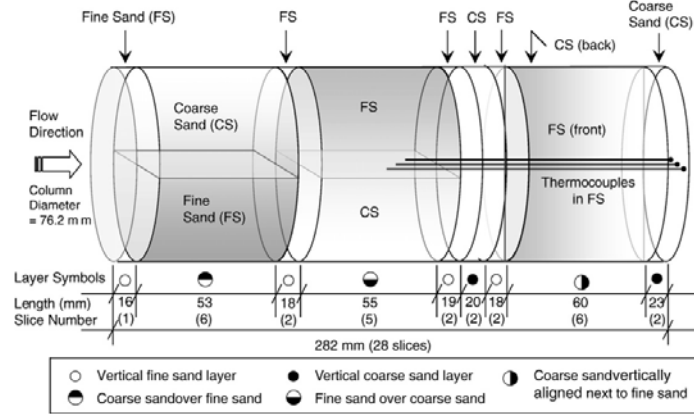
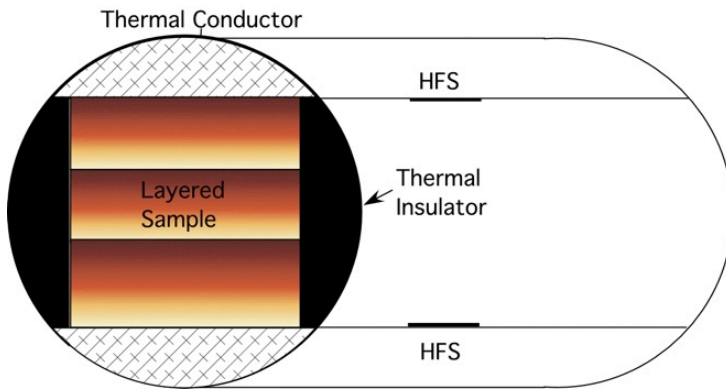


Figure 7. Hydrate formation in a multi-layered sand. Top – configuration of the sand layers in axis transverse and parallel layers of fine and coarse silica sand, and an X-ray CT image of the resulting hydrate configuration formed using the excess gas method in the sand (Seol and Kneafsey, 2009).

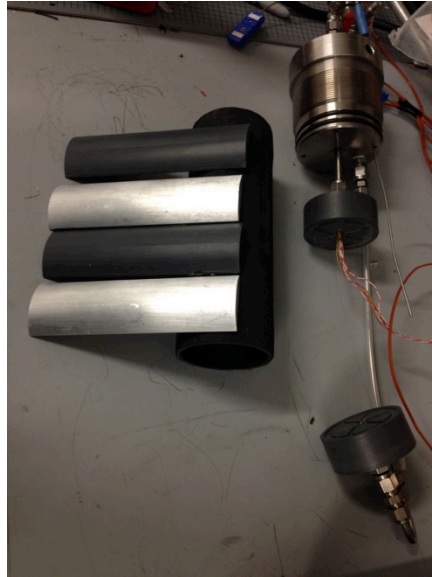
Motivated by these observations, tests in layered systems were performed and reported on in an International Conference on Gas Hydrate paper (Kneafsey and Borglin, 2017), included as Appendix A and summarized below.

### 3.1 Seven-layer system

A seven-layer system was constructed using fine sand and a sandstone having lower porosity and permeability. The conceptual model for the test is shown in Figure 8a. Conceptually heat transfer in a natural layer-cake hydrate deposit would mostly be from the top and bottom boundaries, thus high thermal conductivity aluminum “rounds” were used at the top and bottom, and more insulating low thermal conductivity PVC rounds were used on the sides. Heat flux sensors (HFS) were placed on 3 sides to attempt to understand heat flow in the system. The heat flux sensors contain independent thermocouples as well, and a thermocouple was placed outside the elastomer jacket to provide another indication of heat transfer if a temperature difference occurred.

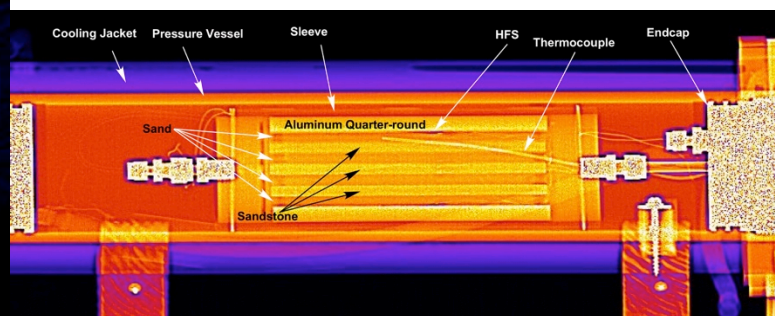
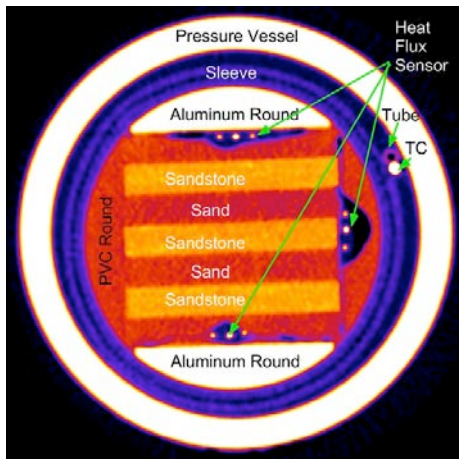


a. b.



c.

d.



e.

f.

Figure 8. a. Layered sample geometry, b. Berea Sister rock slabs (note visible heterogeneity), c. vessel internals including aluminum and PVC “rounds”, and d. end cap showing the passing of wires from thermocouples and heat flux sensors, and e. cross sections of assembled test system.

The layered sample was first saturated with water and then drained vertically allowing methane gas to fill available porespace. This resulted in saturation gradients throughout the sample. Hydrate was formed using the excess gas method, and following hydrate formation the system was resaturated with water. Finally, the hydrate was dissociated. Pressure and temperature were continuously monitored, the density distribution was measured and visualized using X-ray computed tomography (CT), in addition to attempting to measure horizontal and vertical heat flux.

Hydrate formation began in the coarser sand with larger pores. The sandstone layers with the smaller pores remained largely water saturated upon drainage, however some locations drained partially. Because of this, the concentration of methane in the water in the tight sandstone layer would be governed by diffusion through the water. This would result in a gradient that would favor hydrate formation on the outside of that layer. Where hydrate forms, it consumes liquid water resulting in solid material in the pores, reducing the effective pore size. In a partially saturated system, this pore size reduction causes water to flow *towards* hydrate formation from somewhere else (see discussion above related to Seol and Kneafsey (2009)). From this experiment, our observations are that *hydrate formation caused local capillary pressure gradients that induced water to flow towards the hydrate from both the coarse sand layer, and also from the tighter sandstone*. Thus, the partially hydrate-filled pores in the coarse sand became smaller than the hydrate-free pores in the sandstone. This resulted in partially draining the sandstone which provided the opportunity for hydrate to form there.

Because our system had relatively high permeability, the effect of depressurization was experienced throughout the sample almost instantaneously. *Hydrate dissociated throughout the sample, with the longest lasting hydrate being present in the initially highest water saturation regions in the coarse sand*. Prior to the experiment, we did not expect hydrate formation to occur in the sandstone, yet it formed and began dissociation immediately on depressurization. In the initially dryer regions, the hydrate formed on the faces of the sandstone (near access to water), whereas in the wetter regions, the hydrate eventually formed throughout the sandstone.

Because of the heterogeneity of the hydrate formation, the placement of the heat flux sensors containing thermocouples were not ideal. It is not clear how the different thermal conductivities of the PVC and aluminum “rounds” affected hydrate formation and dissociation. Hydrate formation was strong at the top and bottom where the high thermal conductivity aluminum rounds were, but the PVC “rounds” did not seem to hinder or help either formation or dissociation. *The heterogeneity of the initial water saturation was a much stronger driver of system behavior*. The effects of small gradients in expected capillary pressure due to heterogeneity and anisotropy in the natural rock or in packing have not been investigated yet (see Figure 6 for preliminary work), but are likely to strongly affect overall system behavior. There is a structure in the hydrate dissociation locations and this can be compared to the initial porosity and water saturation distributions.

Heat flux sensors used in this test did not provide adequate data to quantify heat transfer in this system. The thermocouple in each sensor functioned as expected, however the HFS did not. The HFS are composed of a number of thermocouples placed on either side of a material of known thermal conductivity (here Kapton). The thermocouples are placed in series to provide a larger signal than a single thermocouple. A number of things could have caused malfunction. The first is water. These devices are manufactured for normal use while dry. Our system required not only submersion, but submersion under pressure. Although we took extensive precautions by epoxying the connections (Kapton and Teflon are difficult to epoxy and special epoxy was used), any leak into the HFS could partially short a portion of the thermocouples, overwhelming the comparison of signals from the two sides.

### 3.1.1 Seven-Layer Test Conclusions

Layered systems are very important in natural gas hydrate systems and in the production of gas from gas hydrate. This study has shed some light on gas hydrate dissociation in an anisotropic medium with a mild capillary entry pressure differential. This sequence of tests provides insight into the interplay of capillary forces, heat flux, and hydrate formation and dissociation. Other studies, such as the study by Seol and Kneafsey (2009) and Rees et al.(2011) provide additional information on layered systems. In these studies, the contrast in capillary entry pressure was mild, and the structural integrity of the sample was sufficient (although a hydrate-formation induced fracture was observed in the earlier study). Natural systems containing higher property contrasts including sands and muds are being studied to observe the magnitude of processes of concern, particularly geomechanical and flow processes. Some of these studies as part of a USDOE/KIGAM collaboration are presented elsewhere.

## 3.2 Technique development for sand/mud layered systems

To investigate the behavior of layered sand/mud systems which are present in many locations in the world and which approach the behavior to model other similar systems (turbidite sand systems) laboratory techniques were developed to create such samples. Since most tests on pressurized samples are performed in cylindrical systems and flow parallel to the layers is needed, a technique was developed that allowed such samples to be created. Creating a sample within a tube from the end would result in compaction in the direction perpendicular to that formed by nature. Thus a new technique was needed. The fundamental idea is modified from Oyama et al, 2016 . In the technique, two hemi-cylindrical molds (Figure 9) were manufactured to the dimensions of the desired sample to fit into the elastomer sleeve. Each mold was used to create one half of the sample. For example, a stiff mud with specific qualities and formulation can be compacted in one half, on top of a plastic film. The stiff mud samples typically have good cohesion and can be carefully removed from the mold. Moist sand can be compacted in the other mold. Unfortunately, the sand samples do not have good cohesion and the samples were frozen to hold them together. When needed, the mud was frozen as well. When removed from the molds, the two halves are assembled and carefully slipped into an elastomer sleeve and endcaps placed at the ends. When this assembly is placed into a pressure vessel and once the samples thawed, a confining pressure can be applied to compact the samples. This technique was

extensively used in a collaborative project between the USDOE and KIGAM, and that is reported on separately.

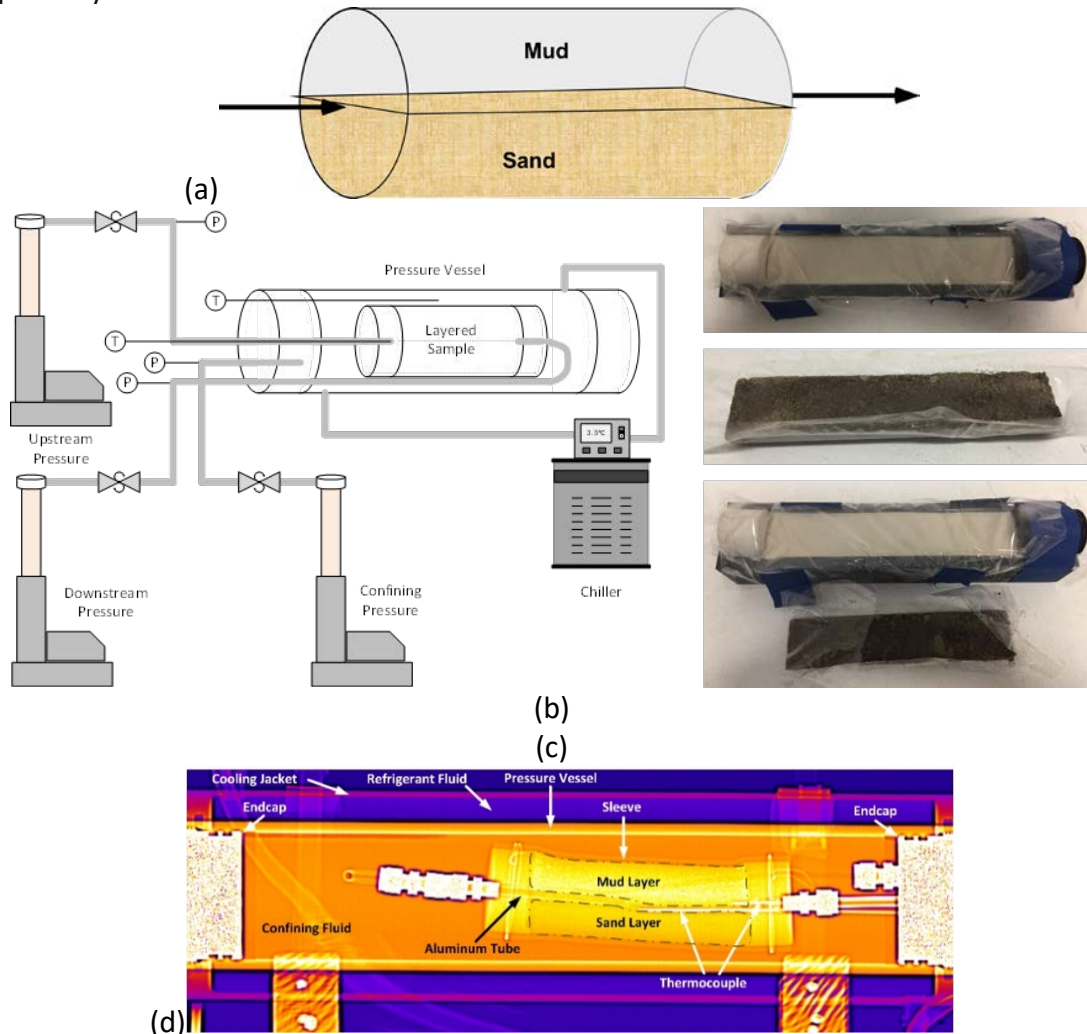


Figure 9. (a) Layered sample test schematic. (b) schematic diagram of the experimental setup, (c) packed mud/sand layer in molds prior to sample packing, and (d) CT image of packed sample after pressurization. Compaction of the mud layer results in the upward curvature of the sample.

### 3.3 Summary, Interpretation, and Conclusions

The presence of varying properties imposed by layers strongly impacts the behavior of hydrate-bearing systems. The ability to study these in the laboratory is critical so that the effects of the layers can be sufficiently considered in numerical models. The location of hydrate formation, dissociation, gas flow, and water flow will all be different than in “homogeneous” medium. Although the systems observed were somewhat weakly anisotropic, under excess gas conditions, hydrate tended to form in the less water-saturated sand, and when the capillary suction of the hydrate-bearing coarse layer exceeded the capillary suction of the non-hydrate-bearing finer layer, the water was extracted from the finer layer and hydrate formed in both. Upon dissociation

by depressurization, the pressure diffusion was rapid across the sample and hydrate dissociated everywhere with the most hydrate-saturated coarse sand taking the longest to dissociate.

## 4.0 Theme 4. Vessel modification

**Theme objectives:** Redesign LBNL X-ray transparent pressure vessel to allow for two entry and exit ports that are required for each phase on each end to allow simultaneous addition and withdrawal of fluid at each end of the sample. Additional modifications were needed to maintain a desired concentration gradient.

In this task, a number of methods were investigated to develop and control thermal gradients. Earlier work resulted in the addition of a 1/8 inch stainless steel coil passing through the endcap (Figure 10 top left). This coil extended to near the sample, and chilled or heated water was flowed through the coil to change the temperature distribution. There were several problems with this embodiment. The first was that the tubing was too small to rapidly flow chilled or heated water through. The second was that the stainless steel causes excessive artifacts in the X-ray images thus could not be extended farther into the vessel. The third was the development of thermally induced circulation in the confining fluid.

To address the possibility of thermal convection, the viscosity of the confining fluid was significantly increased using gelatin. This has a number of effects on testing. The most obvious is that it does solve the thermal convection problem. Even dilute gelatin behaved as a solid for the purposes of reducing convection. This aids in sealing the vessel as well, as the high viscosity material does not leak easily either out of the vessel or into the sample. On the other hand, the semisolid confining fluid adds complications in setup and cleanup of the tests.

To create a temperature gradient, the first change we had to make was in quantification. We attempted to use a single thermocouple swaged using Teflon ferrules and sliding the thermocouple axially through the pressure vessel. This method appeared to work fine, however at one point, we noticed that the thermocouple was being extruded under fairly low pressure. We then instrumented the vessel more carefully.

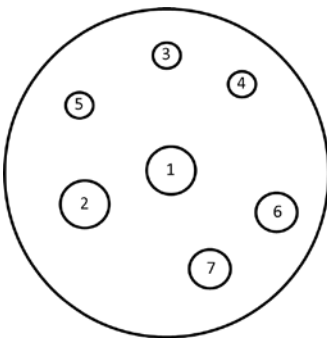
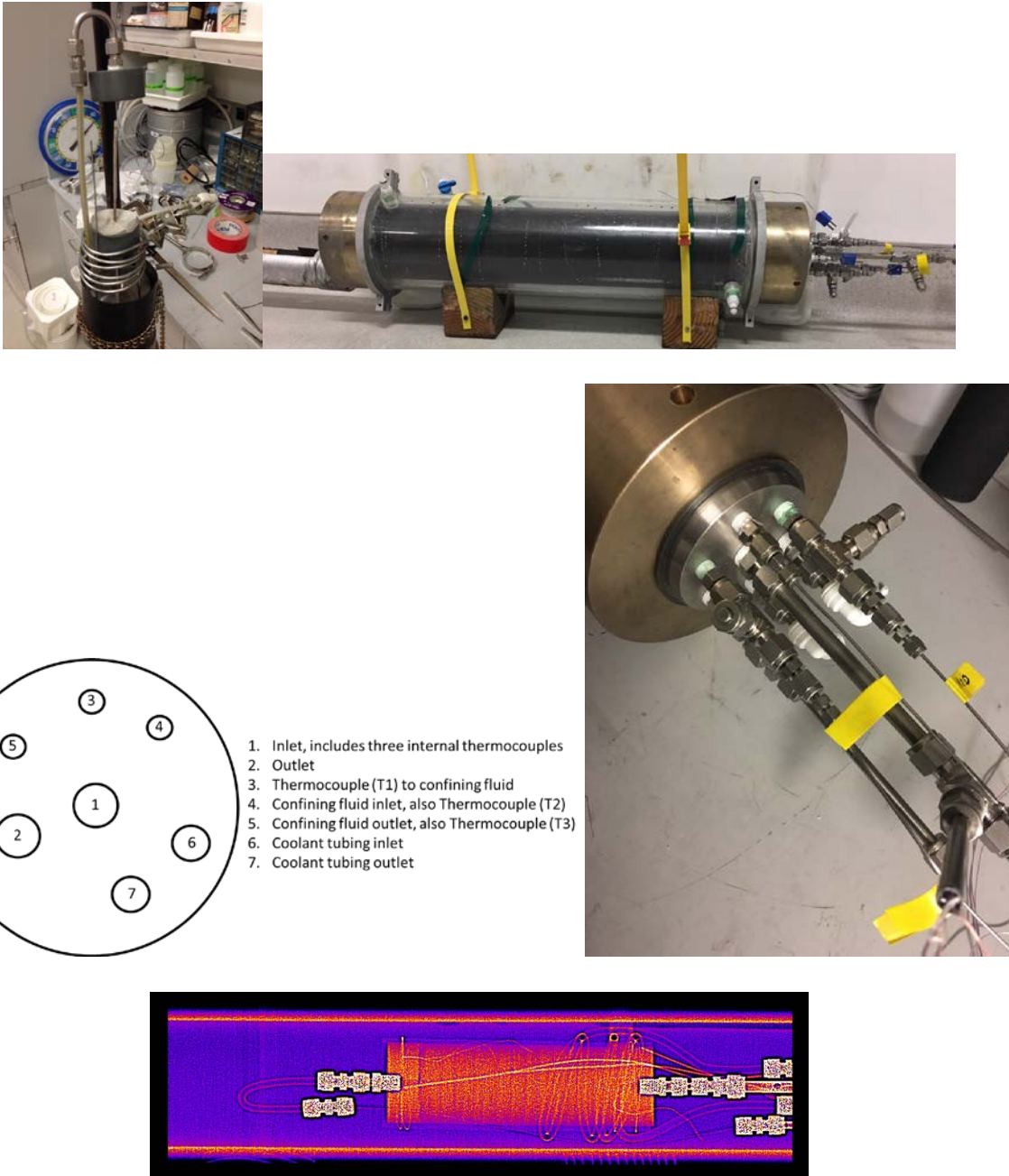
We attempted the use of a wire heater element inside the stainless steel coil. Although conceptually easy, we had difficulties obtaining a wire heater that had high enough output and met the electrical safety requirements at LBNL. The wire heaters that were tried were not effective, thus we abandoned the method.

### 4.1 New X-ray transparent vessel

For a number of reasons including ability to apply a temperature gradient, we designed a new X-ray transparent pressure vessel, found outside vendors, and had the vessel manufactured. The new vessel has a larger internal diameter than the previous one allowing larger samples to be examined, and a longer length as well (Figure 10). In addition, seven larger feedthroughs were placed on one endcap. This allows flexibility on implementing instrumentation within the vessel.

Upon completion of setting up the new vessel with new larger diameter aluminum X-ray transparent coils, temperature gradients were induced in hydrate-bearing samples. The fundamental reason for applying the temperature gradient is that there are very natural

temperature gradients in nature, and while producing gas from hydrate, including the possibility of secondary hydrate formation. This work is described in Theme 5 below.



1. Inlet, includes three internal thermocouples
2. Outlet
3. Thermocouple (T1) to confining fluid
4. Confining fluid inlet, also Thermocouple (T2)
5. Confining fluid outlet, also Thermocouple (T3)
6. Coolant tubing inlet
7. Coolant tubing outlet

Figure 10. top left – inadequate heater coil, top right – new pressure vessel and cooling jacket, middle left – schematic of feedthroughs on one endcap, middle right – all feedthroughs instrumented and in use, bottom – X-ray scan of a hydrate-bearing sample in the new vessel. The coil on the right is much larger than the original, and X-ray transparent.

## 4.2 Summary

A new custom X-ray transparent pressure vessel allowing testing large samples and the application of temperature gradients and multiple sensors has been manufactured and put into operation. The vessel has a maximum allowable working pressure of 2000 psi, an inside diameter of just under 4 inches, an inside length of 20 inches, and is designed to operate over the temperature range of -10°C to 60°C. The pressure range will allow investigation of methane hydrate at temperatures up to almost 15°C.

## 5.0 Theme 5. Thermal Gradients/Chemical Gradients/Well Analogs

**Theme objectives:** Investigate hydrate behavior in the presence of gradients that are present in nature or in producing systems – chemical, temperature, and pressure.

### 5.1 Impact of a chemical gradient

In a hydrate bearing system where salinity is a factor, the formation and dissociation of hydrate will affect the salinity, and the salinity will affect the equilibrium conditions (Figure 11). The hypothesis tested is: Rapidly dissociating hydrate will follow the pure water equilibrium curve, whereas in a slowly dissociating system, hydrate will follow a salty equilibrium curve BECAUSE there is adequate time for salt transport (advection, diffusion, osmosis) to occur in the slow system but not the fast system (Figure 11) unless the dissociation stirs the system making the water film thin.

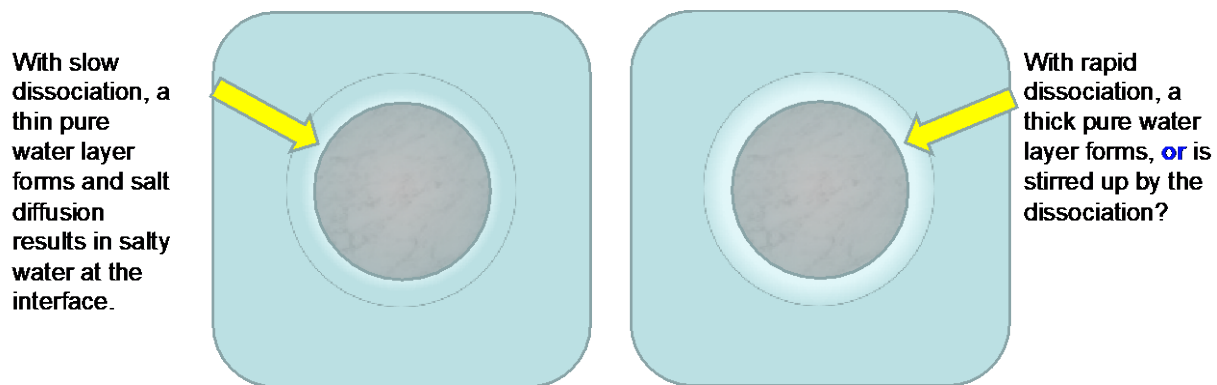
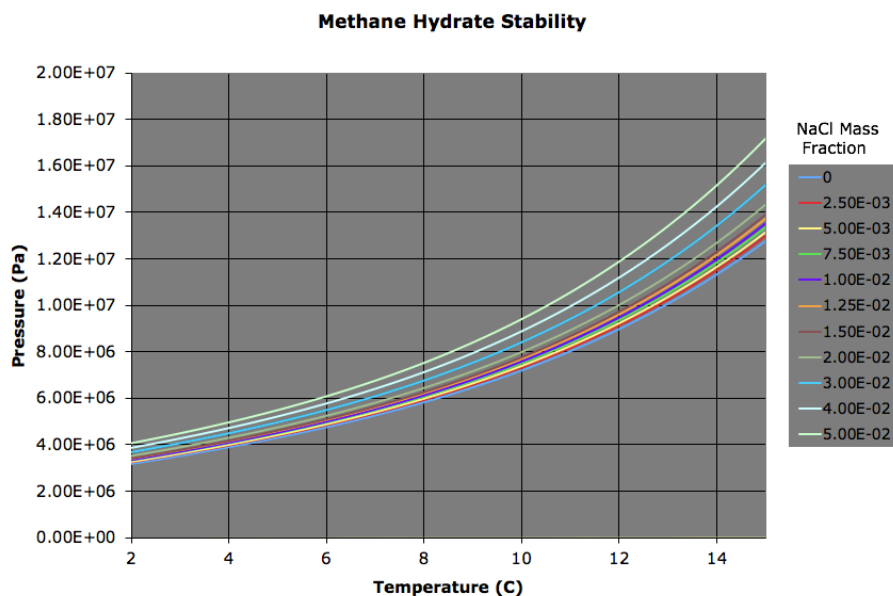


Figure 11. top - Methane hydrate equilibrium curves incorporating the effect of salinity. bottom – schematic of processes occurring during slow (left) and fast (right) dissociation.

Analog tests were performed to investigate phase behavior. In these tests, ice was used as the analog for hydrate, and the liquid phase was a sodium chloride brine, and several kinds of tests were performed (Figure 12). These included tests with floating chipped ice, floating solid ice (chunk), and solid ice on top of a porous medium to reduce mass transfer. With the brine/ice systems, both stirred and unstirred cases were considered. Stirred tests would provide faster mass transfer than unstirred, chipped ice would provide a larger mass transfer area than solid ice, and sand in the brine would slow mass transfer significantly. There are still several considerations. Brine is more dense than water at constant temperature, however it is possible to have higher-density-lower-salinity brine with a temperature gradient. This might induce convection in unanticipated directions. Therefore temperature is always important, and the presence of isothermal conditions does not necessarily indicate that chemical gradients will not induce convection.

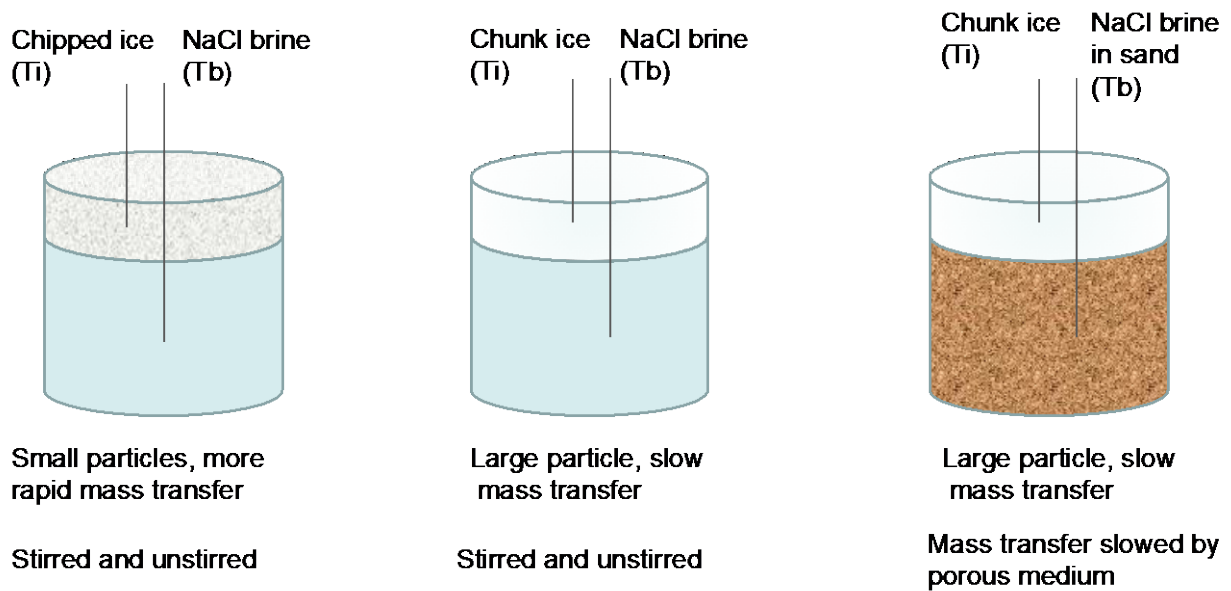
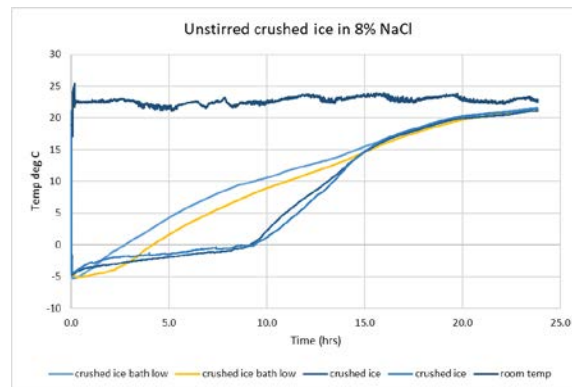


Figure 12. Test configurations for hydrate dissociation analog tests. Left – crushed ice in brine, middle – solid ice in brine, and right – solid ice over brine-saturated sand.

Examples of the test results are shown in Figure 13. In these examples, temperatures were measured in the ice zone, below the ice zone in the bath or brine, and often in an external location.



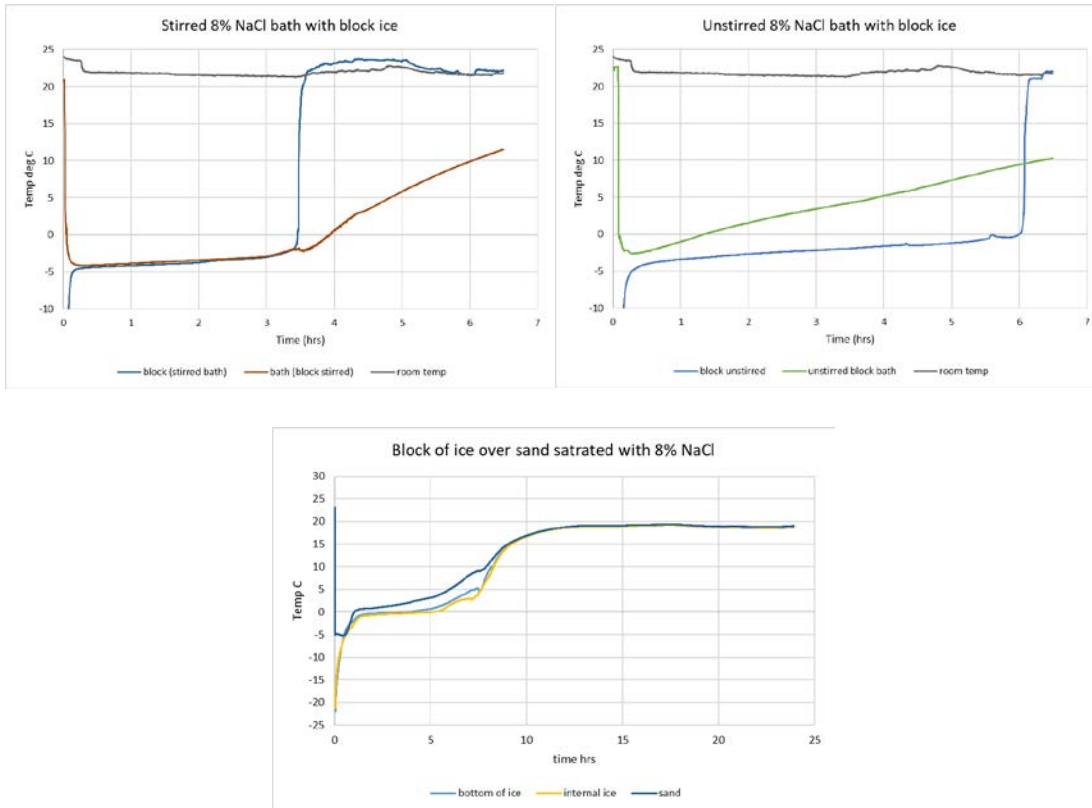


Figure 13. Recorded temperatures for three of the 12 experiments. top – unstirred test with crushed ice, middle – stirred and unstirred tests with solid ice, and bottom – unstirred test with block ice and sand in the brine.

In the top panel of Figure 13, the two blue curves indicating the temperature of the fluid in the crushed ice region remain significantly below zero for about 10 hours while the temperature of the brine below warms past the normal ice melting point. These results indicate that initially the thawing is at the brine-influenced temperature. The influence of the salt decreases over time as the ice melts. This is consistent with the hypothesis. The test was problematic, however in that the temperature of the ice itself was not quantified and the temperature of the brine was. In the middle panels of Figure 13, the block of ice in the stirred brine thaws well below the normal ice melting point. In this case, the ice is always in close connection with brine, and no thick pure water layer is formed. This indicates that the salt water constantly affects the thawing temperature. In the unstirred brine, the ice also melts closer to but still well below the normal melting point. This indicates that there is significant mass transfer in the sub-ice brine, possibly from convective currents caused by mixing of the dilute and less dilute brine. This is also consistent with the hypothesis. In the bottom panel of Figure 13, a block of ice was thawed over brine-saturated sand. Any flow in this brine would be hindered by the presence of sand. In this case, the ice melts at 0°C. This is also consistent the hypothesis. Although verification in a hydrate-bearing system was strongly considered, this was not performed because of the somewhat uncontrolled hydrate formation and need for accurate placement of sensors.

Interpretation: **Where mass transfer is rapid and the ice (or hydrate) is bathed in brine, the melting (or dissociation) will occur at the saline equilibrium melting point (dissociation point). Where mass transfer is moderately hindered (e.g. the unstirred solid ice case) the melting (or dissociation) will occur between the saline equilibrium melting point (dissociation point) and the normal (salt-free) melting (dissociation) point. When mass transfer is slowed further (sandy system), the melting (dissociation) occurs initially at the at the saline equilibrium melting point (dissociation point), and continues at the normal (salt-free) melting (dissociation) point. In a natural hydrate-bearing system, the dissociation pressure and temperature will be affected by the configuration of the system as well, because that will affect the flows of the various fluids.**

## 5.2 Impact of a Temperature Gradient

Temperature gradients are naturally present and could be induced by gas production in the subsurface induced by endothermic hydrate dissociation or exothermic hydrate formation. As temperature is a key variable in hydrate location, and the changes in the temperature gradient relative to the hydrate strongly affect its behavior, it is important to be able to manipulate this experimentally. Geologically, as the suboceanic sediments compact, hydrate-bearing media sink into a warmer environment where the hydrate is unstable. This is a slow process, and although we don't replicate the time scale in the laboratory, it is not needed to do so as the ability of hydrate to adapt to applied conditions is *much* faster than the sedimentation process. It is thought that most attempted isothermal tests have had slight temperature gradients, however they have not been quantified, and it is likely that the effects were small relative to the other processes measured.

As mentioned in Theme 4, a new vessel was constructed to impart temperature gradients in samples. Gelled confining fluid and a large X-ray-transparent heating coil were used to alter the temperature in an otherwise relatively constant temperature sample. The purpose of the gelled confining fluid was to eliminate thermal convection of the confining fluid as a result of any other heat source or sink including the applied heat source. Thus, heat transfer in the confining fluid is primarily conductive rather than convective.

Demonstration of the temperature gradient is presented in Figure 14. The top panel, shows 5 temperatures within the vessel over 2 days. Although there is some temperature variation which may be due to calibration offsets of the thermocouples, the temperatures are within a +/- 0.1C range. As these are raw values, this error is acceptable. The middle panel shows temperatures at the same locations over one day time under the application of a temperature gradient. These temperatures show a range of approximately 1C. The methane hydrate equilibrium pressures at these temperatures span about 65 psi. Pressure and temperature are both easy to control in the lab, but pressure response is generally very rapid and temperature change is often slow. Thus a temperature gradient can be applied across a sample entirely under equilibrium conditions and pressure control can move the equilibrium front accurately. Additionally, temperature and temperature gradient oscillations can be applied as well allowing multiple gradients to be investigated. This was not the intent of the measurements in the bottom panel of Figure 14, however the data show this. It was intended to cycle the oscillation much more slowly, akin to tides.

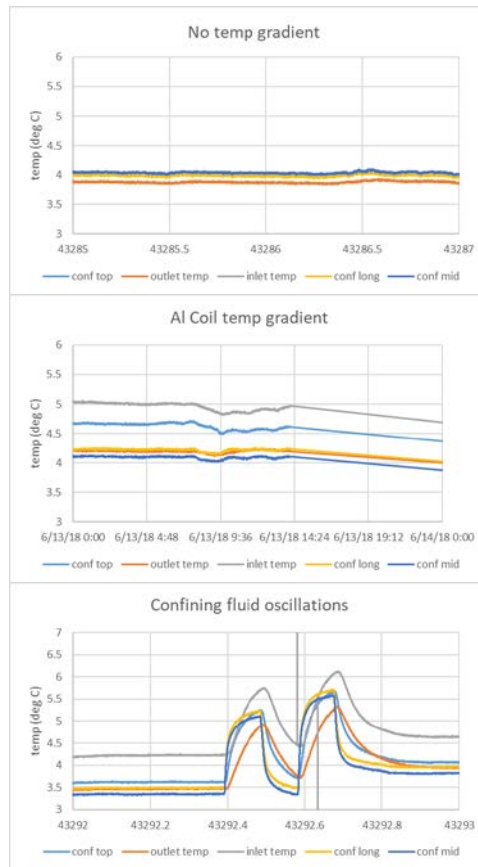


Figure 14. Demonstration of temperature gradient in a sample in the new vessel. top – fairly uniform temperatures in the sample, middle – strong temperature gradient (1°C over 15 cm) (see vertical spacing of temperature signals), bottom – oscillating temperatures and temperature gradients.

Figure 15 shows the behavior of a hydrate-bearing system in response to the application of a temperature gradient to a system containing methane hydrate. The top panel shows an X-ray CT cross section of a hydrate-bearing sand. This hydrate was formed using the excess gas method and is somewhat nonuniform. In the image, the packing layers are clearly seen. The higher density regions indicated by the brighter colors depict the location of the hydrate. Also seen in the top panel are 6 white circles. These are cross sections of the aluminum tube which extends through the end piece of the vessel in which chilled or heated water is flowed. The second panel shows the result of applying the temperature gradient with a warmer fluid. The hydrate in the right side of the sample dissociated, and both the water and gas migrated to the left, resulting in a mass of hydrate across the sample. In the third and fourth panels, the pressure was lowered slightly resulting in some mass being removed from the system, but also in the hydrate mass moving more and more to the left. Upon reducing the temperature gradient so that the equilibrium moved to the right, some hydrate re-formed in the previous location, however the mass in the middle of the sample remained.

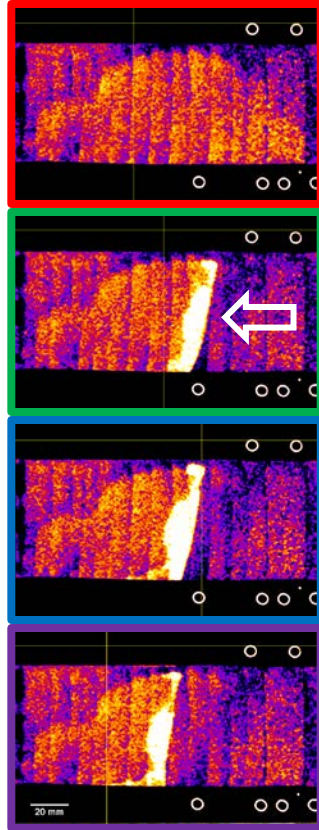


Figure 15. Changes in hydrate-bearing sample as a result of an applied temperature gradient. The right region was slightly warmed, resulting in hydrate dissociation, water migration to the left and hydrate formation where the sample remained in the hydrate stability envelop. As the right was warmed, the process continued and the highly saturated hydrate-bearing zone was moved to the left. Reducing the system pressure caused the hydrate to move to the left (cooler), and cooling the right resulted in some hydrate forming there but does not result in redistribution to the original state.

### 5.3 Impact of Pressure Gradients - Horizontal/Vertical Well Analogs

Flow to horizontal and vertical wells will result in different pressure gradients in the subsurface. For the same production, a vertical well penetrating a thin hydrate bearing later will need to exert a much larger pressure gradient, than a horizontal lateral that is in a hydrate bearing layer. These differences might affect other behaviors, for example secondary hydrate formation has been predicted due to Joule-Thomson affects for large pressure gradients towards a vertical well. The flow of sand may be different as well. Although these two systems would be produced differently, a comparison is justified (Figure 16).

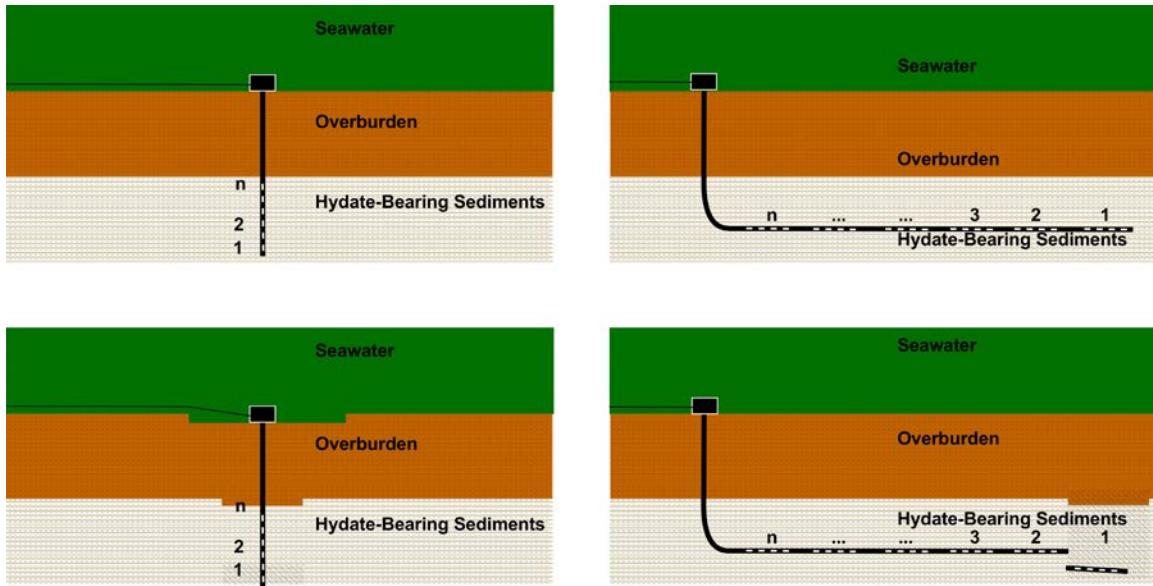


Figure 16. left - vertical and right – horizontal wells. Top – without geomechanical failure, bottom – with failure and the horizontal well operated in sections.

We performed a number of tests to model a hydrate-bearing sand under various conditions. These include:

1. hydrate-bearing
2. low water flux
3. high water flux
4. open well
5. screened well

All tests were performed with moderate effective stress (150 – 200 psi). The purpose of the moderate effective stress is to hold the sand grains together.

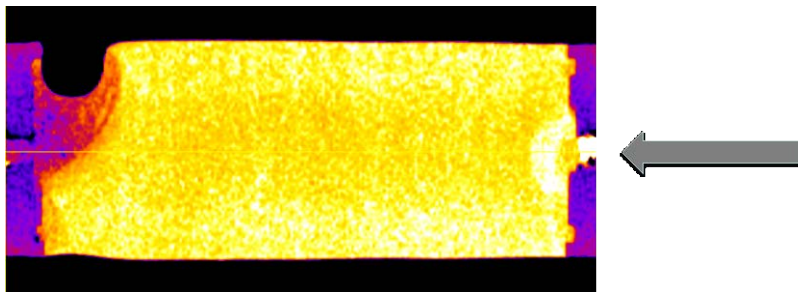


Figure 17. X-ray CT cross section of a sample without sand control. Note the caving of the sample on the left top of the sample.

In spite of all the conditions investigated, a single conclusion can be drawn. ***ALL sand samples failed unless the sand was controlled at the well.*** This is consistent with many earlier observations (generally these are considered failed tests and typically not reported) and work as part of a USDOE/KIGAM collaboration presented elsewhere, which used sand/mud layers as well.

## 5.4 Summary, Interpretation, and Conclusions

### 5.4.1. Chemical Gradients

A number of chemical gradients have been investigated over the years including the use of methanol as an inhibitor, gas chemistry, and salinity. The methanol test was not reported as it was considered a failed experiment. In light of the current observations, it deserves mention however. At the end of a series of tests, methanol was injected into a cylindrical partially hydrate-saturated sand sample. The sample was permeable, as gas flow had been performed as part of the tests. The hypothesis for this ad-hoc test was that the methanol would cause hydrate dissociation in the sample resulting in greater permeability. Upon the methanol injection, the sample became impermeable, however, exactly the opposite of the hypothesis. We now interpret this using the results discussed herein. As expected, the methanol induced dissociation as it contacted the hydrate. As with the results of the temperature gradient above, and the brine/ice tests, the newly released water from the dissociated hydrate diluted the methanol, and because the hydrate-bearing sediment has a higher capillary suction than the hydrate-free sediment, the liquid flowed towards it. As the methanol injection progressed, the water was dilute enough in methanol at the front that hydrate could form, creating a blockage similar to that shown in Figure 15.

The chemical gradients examined in the series of tests reported here examined the effect of salinity on the melting (dissociation by analogy) point of ice (hydrate by analogy). The chemistry at the immediate solid/liquid interface strongly impacts the understanding of the dissociation equilibrium. In a stagnant volume containing hydrate and brine, the equilibrium condition will be determined by the salinity of the brine. If the hydrate dissociates slowly, such that flow or diffusion processes keep the solid/liquid boundary bathed in saline water, the equilibrium condition for that salinity will govern. If the dissociation is rapid however and the flow and diffusion processes are slow in relation to the production of fresh water from dissociation, the equilibrium condition will be determined by the fresh water condition.

This is regardless of the volume size. It is important to consider however that on the pore scale, advective flow is hampered by the presence of the medium. At the pore scale however, diffusion is a *fast* process. Considering these two processes, one would expect that the equilibrium conditions would start at the natural brine condition and trend towards the fresh water condition. One process not considered is gas evolution. This process will displace and mix fluids present in the porespace. Because the fluids displaced will have some salt and fresh water is generated from dissociation, this will tend to push the dissociation to occur closer to the fresh water conditions.

### 5.4.2 Temperature Gradients

In hydrate-bearing systems, normal geothermal gradients are always present, and many models account for these. Hypotheses about hydrate behavior as the sediment column sinks are available, however laboratory verification was not. Temperature gradients due to gas production from hydrate would also be expected. The endothermic nature of hydrate dissociation would result in cooling upon dissociation. In addition, in flow, particularly in radial flow towards a

vertical well from a horizontal layer of hydrate-bearing sand, will result in Joule-Thomson effects and additional cooling as gas expands. Numerical studies have indicated that secondary hydrate may form, impacting continued production. Very few laboratory studies have acknowledged or quantified temperature gradients in hydrate-bearing systems. This is primarily because of the added difficulty in making the required measurements.

Our studies, while limited, have shown agreement with sinking sediment conceptual and numerical studies where hydrate is concentrated at the base of the gas hydrate stability zone. Our timescales are very different however, so complete verification has not occurred. Additional testing would now be relatively easy, as such temperature gradient controls and strategies are now available.

#### 5.4.3 Pressure Gradients

Our study of the impact of pressure gradients (modeling horizontal vs vertical well) indicated that the effects on the medium were dominating. Studies by others have shown immense pressure gradients across stable hydrate lamellae (hypothesized but not observed) (Meyer et al., 2018). In this case, it is possible that minor grain rearrangement occurred, however very large pressure gradients developed as hydrate formed.

Over the course of many studies we have performed both under this work package and others resulted in a simple conclusion: the flow of sediment, particularly sand, into the well must be controlled. We saw catastrophic sample failure without sand control. We also saw mud blockage of the well without sediment control in the finer-grain sediment.

## 6.0 Other Activities

Numerous other activities have been performed related to this work package and resulting from work performed as part of this waste package. These include:

1. Participation in an effort to investigate the use of CO<sub>2</sub> hydrate in desalination of produced water. This coordinated effort included professors and students from the Colorado School of Mines, the Petroleum Institute (Abu Dhabi) the University of Western Australia, and a commercial entity.
2. Participation in an effort with the Colorado School of Mines involves investigating equilibrium chemical properties of hydrate/gas or hydrate/fluid systems. This is an ongoing investigation performed by CSM students and postdoctoral researchers at both LBNL and CSM.
3. Participation in an effort with the University of Texas looking at hydrate formation/dissociation, experiment design and monitoring, under three-phase equilibrium conditions.
4. Recent conference session leadership
5. Session chair: ICGH9
6. Session lead and coordinator: Gordon Research Conference
7. Discussion Leader 2016 AGU Fall Meeting - The status and direction of hydrate research - a discussion
8. Session Chair and Discussion Leader 2015 AGU Fall Meeting

## References

KNEAFSEY, T. J. & BORGLIN, S. E. 2017. Experimental Observations of Methane Hydrate Dissociation in Layered Media. *9th International Conference on Gas Hydrates*. Denver CO.

Oyama, H., S. Abe, T. Yoshida, T. Sato, J. Nagao, N. Tenma, and H. Narita (2016), Experimental study of mud erosion at the interface of an artificial sand-mud alternate layer, *Journal of Natural Gas Science and Engineering*, 34, 1106-1114, doi:<http://dx.doi.org/10.1016/j.jngse.2016.07.067>.

REES, E. V. L., KNEAFSEY, T. J. & SEOL, Y. 2011. Methane Hydrate Distribution from Prolonged and Repeated Formation in Natural and Compacted Sand Samples: X-Ray CT Observations. *Journal of Geological Research*, 2011, Article ID 791815, 15 pages.

SEOL, Y. & KNEAFSEY, T. J. 2008. Fluid flow through heterogeneous methane hydrate bearing sand: observations using x-ray CT scanning. *6th International Conference on Gas Hydrates (ICGH 2008)*. Vancouver, British Columbia, Canada.

SEOL, Y. & KNEAFSEY, T. J. 2009. X-ray computed-tomography observations of water flow through anisotropic methane hydrate-bearing sand. *Journal of Petroleum Science and Engineering*, 66, 121-132.

## Hydrate Papers/Presentations from LBNL Lab

- Borglin, S. E.; Kneafsey, T. J.; Nakagawa, S., Methane hydrate behavior when exposed to a 23% carbon dioxide 77% nitrogen gas under conditions similar to the ConocoPhillips 2012 Ignik Sikumi Gas Hydrate Field Trial, American Geophysical Union, Fall Meeting 2013, abstract id. H51L-1368
- Dai, S., Santamarina, J.C., Waite, W.F. and Kneafsey, T.J., 2012. Hydrate morphology: Physical properties of sands with patchy hydrate saturation. *Journal of Geophysical Research: Solid Earth*, 117(B11): B11205.
- Han, G., T. H. Kwon, J. Y. Lee, and T. J. Kneafsey (2018), Depressurization-Induced Fines Migration in Sediments Containing Methane Hydrate: X-Ray Computed Tomography Imaging Experiments, *Journal of Geological Research - Solid Earth*, 123(4), 19.
- Kneafsey, T.J. and G. J. Moridis (2014). "X-Ray computed tomography examination and comparison of gas hydrate dissociation in NGHP-01 expedition (India) and Mount Elbert (Alaska) sediment cores: Experimental observations and numerical modeling." *Marine and Petroleum Geology* 58, Part A(0): 526-539.
- Kneafsey, T.J., The status and direction of hydrate research – a discussion (Invited), 2016 AGU Fall Meeting, San Francisco, CA, 12-16 December 2016, edited.
- Kneafsey, T.J. et al. Observations of Methane Hydrate Dissociation in Layered Media, in *9th International Conference on Gas Hydrates*, edited, p. 8, Denver, CO
- Meyer, DW, P.B. Flemings, D. DiCarlo, K. You, S.C. Phillips, and T.J. Kneafsey, Experimental investigation of gas flow and hydrate formation within the hydrate stability zone, (2018) accepted, *Journal of Geophysical Research*.
- You, K., Kneafsey, T.J., Flemings, P.B., Polito, P., & Bryant, S.L. (2015). Salinity-buffered methane hydrate formation and dissociation in gas-rich systems. *Journal of Geophysical Research: Solid Earth*, 120(2), 643-661. doi: 10.1002/2014JB011190

## Appendix A - Experimental Observations of Methane Hydrate Dissociation in Layered Media

Kneafsey, T. J., and S. E. Borglin (2017), Experimental Observations of Methane Hydrate Dissociation in Layered Media, in *9th International Conference on Gas Hydrates*, edited, p. 8, Denver CO.

# Experimental Observations of Methane Hydrate Dissociation in Layered Media

Timothy J. Kneafsey\* and Sharon E. Borglin  
*Lawrence Berkeley National Laboratory, United States*

\*Corresponding author: tjkneafsey@lbl.gov

## Abstract

The nature of a porous medium affects gas and water transport, hydrate formation, gas and hydrate distribution, pressure diffusion, and hydrate dissociation. Few studies of layered hydrate-bearing sediments have been performed, and understanding processes affecting flow and mechanics in these systems is important to facilitate gas production from natural layered geologic systems. Following earlier experiments in layered and heterogeneous samples, we have performed a laboratory experiment in a layered sandstone/sand system. In this test, a seven-layer system was constructed using fine sand and a lower porosity and permeability sandstone. Hydrate was formed using the excess gas method, and the system was resaturated with water. Finally, the hydrate was dissociated, while attempting to measure horizontal and vertical heat flux and measuring density distribution using X-ray computed tomography (CT). The CT measurements provide a three-dimensional mapping of electron density in the sample, which is correlated to physical density. This helps in understanding the distribution of water, gas, and hydrate during the tests. Although no mechanical effects were observed in this test, tests are under way to examine physical and geomechanical changes in more complex layered systems, and the effect of dissociation on mechanical properties. In addition, the mechanical effects caused by dissociation and gas production on fines and fines mobility are being examined. Analysis using conventional mass balance approaches and three-dimensional numerical modeling is under way to extend laboratory observations and to build confidence in the simulation process.

## Introduction

Hydrate in nature often exists in layered systems such as turbidite sands in the Nankai Trough or sand layers at Mount Elbert (Colwell, Matsumoto et al. 2004, Collett, Lewis et al. 2011, Kneafsey, Lu et al. 2011). Most laboratory and simulation work has been performed on somewhat homogeneous formations, or on thick layers. Earlier laboratory tests have shown the importance of layers in hydrate-bearing systems (Seol and Kneafsey 2009). The goal of this test was to examine the effects of small-scale anisotropy on hydrate formation and dissociation. In this test, we packed fine sand between thin layers of sandstone to simulate natural layering. For this test we developed a test apparatus to infer heat transfer to and from the sample both parallel and perpendicular to the bedding. The sample was saturated with water and then drained. Methane hydrate was formed using the excess gas method, and the sample was resaturated with water. Following the resaturation, the hydrate was dissociated by depressurization. Pressure and temperature were monitored, and intermittent X-ray CT scanning was performed to understand water, gas, and hydrate behavior.

## Method

Our experimental concept is shown in Figure 1a. We used 6 mm thick Berea Sister Sandstone slabs (Figure 1b. ~ 45 mD, 21.4% porosity, Kocurek Industries) to represent our fine layers, separated by coarser 6 mm thick layers of US Silica F110 sand (~1 Darcy, 36% porosity). To thermally model horizontally extensive layers thermally, we used solid PVC insulating material “rounds” on the vertical sample boundaries (thermal conductivity 0.19 W/m.K) to simulate no heat flow of a laterally extensive system, and aluminum “rounds” (thermal conductivity 205 W/m.K) on the top and bottom (Figure 1c) to encourage vertical heat flow. Heat flux sensors (HFS, Omega Engineering) were placed on three surfaces to attempt to understand the heat fluxes in a layered system.

To set this test up, we attached small plastic spacers to the sandstone slabs, and the HFSs were placed on the flat sides of the PVC and aluminum “rounds”. This assembly was then placed in the elastomer (EPDM) sleeve attached

to a PVC endpiece. The F110 sand was then poured inbetween the sandstone slabs and vibrated to compact it. Twelve wires (Figure 1c) extend from the three HFSs. Each HFS is composed of a thermopile (a number of thermocouples connected in series on both sides of a polyimide layer) and a local thermocouple resulting in 4 insulated wires from each. Because these sensors were not designed for pressurized systems, they could allow pressurized gas to flow between the metal wire and plastic (Teflon in this case – difficult to epoxy) insulation. An epoxy more suitable for Teflon and polyimide was selected to seal the HFSs where the wires exit primarily to keep water out of the sensors. Compression seal fittings were used to seal the wires. Off-the shelf modules that contain both thermocouple wire and conductors were used. We used pin connectors for the thermocouple wires, and lacquered the final connections with an electrically resistive lacquer and adhesive-filled heat-shrink tubing in hopes of maintaining electrical isolation. This required adding two high-pressure couplings to accommodate the added wiring and connections.

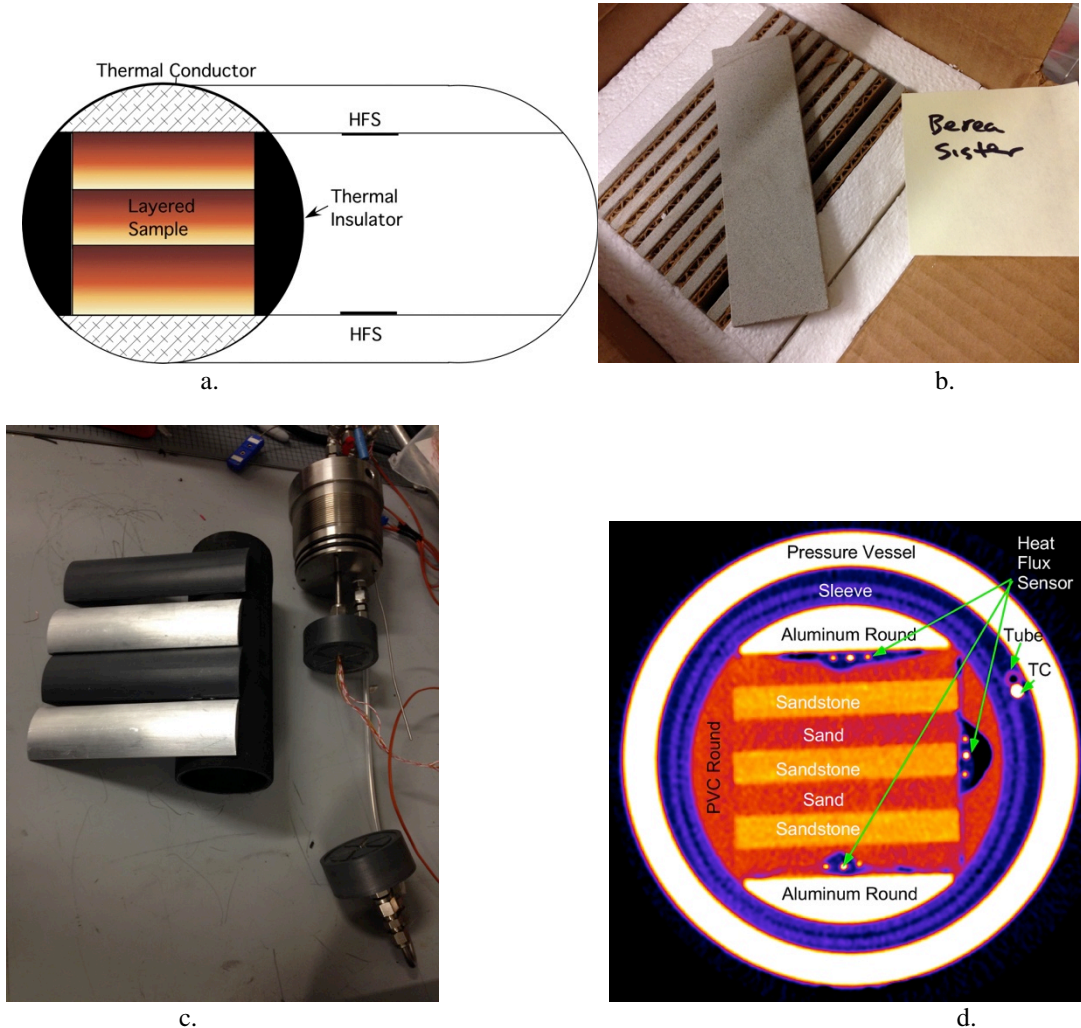


Figure 1. a. Layered sample geometry, b. Berea Sister rock slabs (note visible heterogeneity), c. vessel internals including aluminum and PVC “rounds”, and d. cross section of assembled sample.

Test assembly (Figure 2) was difficult and required numerous repeats of system packing and assembly to achieve proper sand packing, spacer layout, leak elimination, and sleeve seal. Because of the thin wires and rough conditions of the rock and sand, we lost partial functionality of the three of our HFS devices after startup. Once inside the sleeve and both endpieces attached, the sample assembly was placed in an X-ray transparent aluminum pressure vessel filled with a propylene glycol solution. This solution allows the application of a confining stress, controlled using a high-pressure syringe pump. The pressure vessel was placed in a custom temperature jacket allowing it to be bathed in chilled fluid, and the jacket was supported by a pressure vessel stand which oriented the vessel vertically, but allowed the sample to be rotated to the horizontal position for X-ray CT scanning (Figure 2b.). The porosity

computed using CT data averaged transverse to the flow direction is shown in Figure 3. The porosity distribution of the whole sample is shown in Figure 3b. The distribution is bimodal and clearly shows the individual porosity distributions of the two media, with the left peak for the sandstone and the right peak for the sand.

### Hydrate Formation

The air in the sample was evacuated, and the sample was saturated with water and allowed to drain until no more water was produced. After draining the sample, it was placed horizontally for more than two days to equilibrate. The water saturation after drainage is shown in Figure 4. As expected, the water saturation in the tighter sandstone was generally close to saturated and much higher than in the coarser sand. After equilibration, the air in the sample was again evacuated and replaced with compressed methane and the sample was chilled to about 4°C to induce hydrate formation.

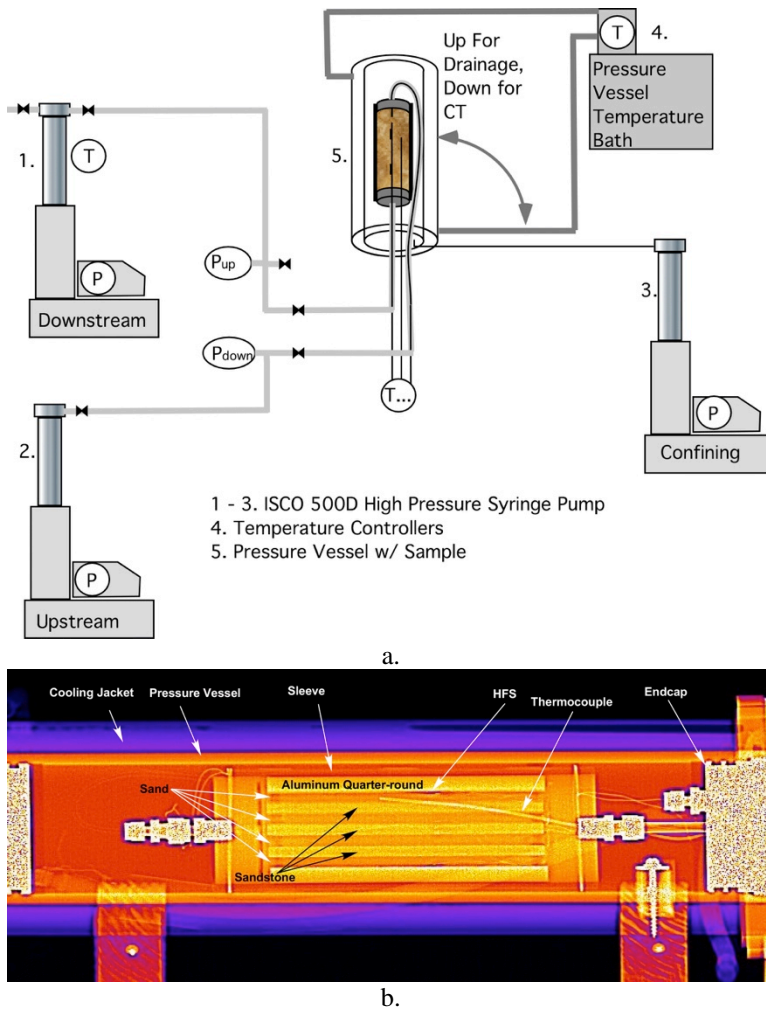


Figure 2. a. System schematic, b. Sample and pressure vessel assembly.

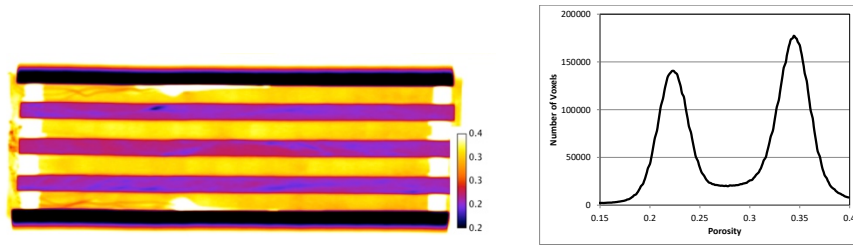


Figure 3. Left - Porosity averaged across the sample transverse to flow. Right – Porosity distribution of entire sample showing expected bimodal distribution from the two sample components.

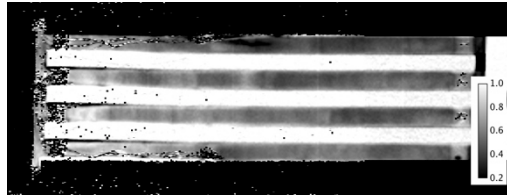


Figure 4. Water saturation at start of hydrate formation. Note that the sandstone slabs (white here) are nearly entirely saturated.

Hydrate formation was documented by frequently collected pressure, temperature, and volume data (Figure 4), and intermittently by X-ray CT. Fifteen sets of CT scans were taken using both 80kV and 120 kV energies (288 slices/energy/scan) in hopes of using the differences between the energies to infer processes. For this sample, the multiple energies were not helpful because of the relatively constant differences in attenuation between 80 and 120kV for the elements in the test. Changes in higher atomic number elements are more readily identified using this technique.

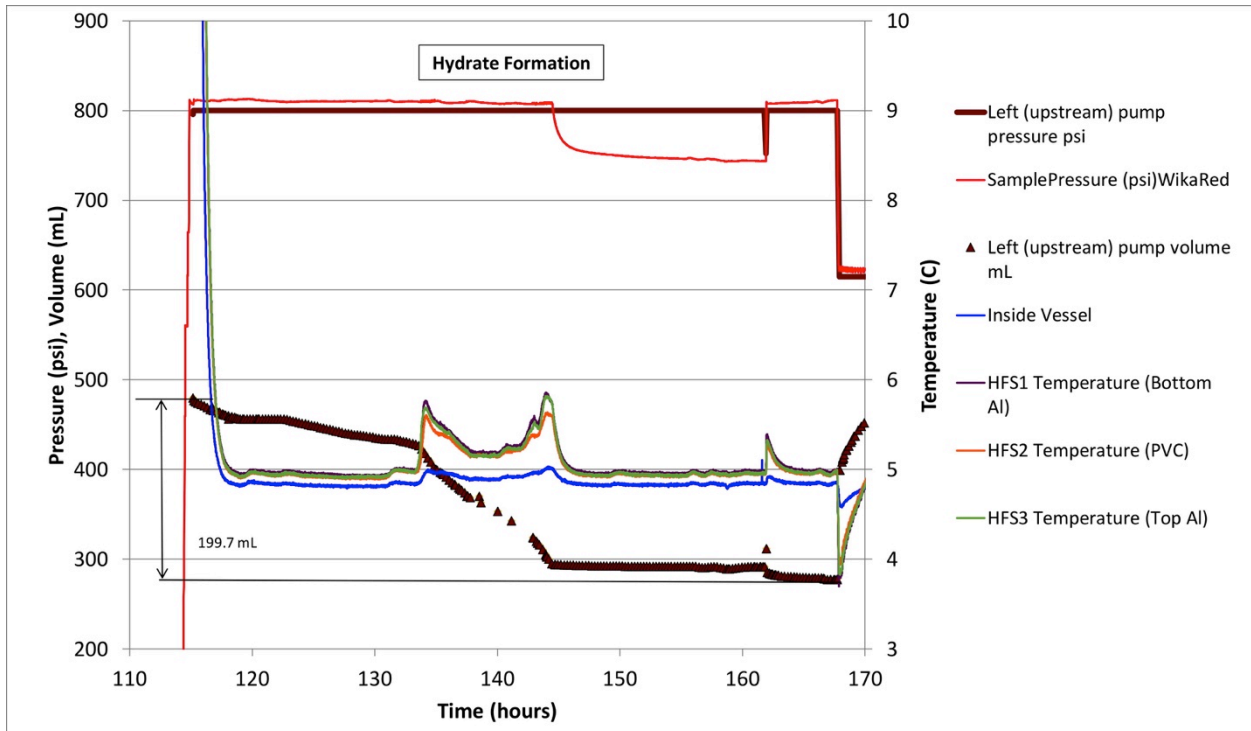


Figure 5. Pressure, temperature, and volume measurements during hydrate formation.

Hydrate formation was identified by a decrease in volume of the constant pressure supply pump and an increase in temperature in the system (between hours 130 and 145, Figure 5). The drop in system pressure between 145 hours

and 160 hours (red curve) was caused by shutting the system in and allowing it to reach a steady pressure. Note that there was a small decrease in the volume of the supply pump, which at the time was independent of the sample, indicating a small leak in the pump. Upon opening the sample to the supply pump, the pressure increased and additional hydrate was formed (~162 hours). Changes in total saturation (total saturation does not distinguish between hydrate and water and assumes all changes are water) are shown in Figure 6. Note that the saturation in the sand became more heterogeneous and clearly increased both as a result of hydrate formation and from absorbing water from the sandstone. In addition to increasing the heterogeneity and patchiness of the hydrate formation, it allows hydrate to form in the sandstone which was previously completely saturated with water.

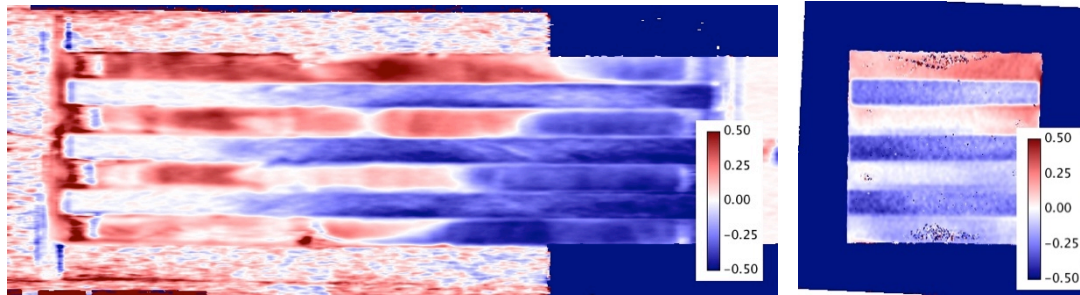


Figure 6. Change in total saturation following hydrate formation

Following hydrate formation, the sample was saturated to the largest extent practical by injecting water. Initially, room-temperature water entered the sample but at a low flow rate, assuming that the water would cool when passing through the 15 cm of cooled tubing at the sample inlet. This may have induced some dissociation, however hydrate formation also occurred making the resaturation difficult and requiring that the flow rate be lowered substantially.

### Hydrate Dissociation

Hydrate was dissociated by depressurization. Prior to dissociation, the pressure was lowered to approximately the equilibrium pressure (first sharp pressure decrease after 189 hours in Figure 7), and the system was allowed to equilibrate briefly. For the depressurization, gas was produced at specific rates, lowering the pressure to about 420 psi, roughly 200 psi lower than the equilibrium pressure at the system temperature. In a uniform system, even an anisotropic system with uniformly distributed hydrate, the expectation would be that the temperature of the HFS on the PVC round would be lower because of the reduced heat transfer compared to the HFSs on the aluminum rounds. A possible explanation for this not being the case is that we can see from Figure 6 that the lion's share of the increase in saturation (hydrate) is present near the top and bottom HFSs, and less near the side HFS where the PVC round was present.

Figure 8 presents the changes in the hydrate-bearing sample over the depressurization. In this figure, the color black indicates very little change, and the white represents a large saturation change. Much of the hydrate is in the coarser sand layers, and the gas exit is on the right in the figure (left pump). If we start at the latest time (lowest image in the figure), there are some regions that had no change. These are regions in the tighter sandstone that had lower saturation following hydrate formation. This indicates that very little hydrate formed there, except for possibly at the interface between layers where water would have remained in the sandstone. The largest initial changes (top of Figure 8) are in the low hydrate saturation zones and at the interface between the sand and sandstone, although there are changes in the tighter sandstone as well towards the center of the sample. In the second set of scans, the pattern is similar to the first, but much more hydrate has dissociated resulting in lower density from the presence of gas. Additionally, towards the left side (away from the gas exit) dissociation reduces the density in the sandstone as well as the sand. The same trend continues over time with each step becoming brighter, except for the last two which are very similar. These observations are consistent with the measurements shown in Figure 7 which show very little change in produced gas volume for the last two scans.

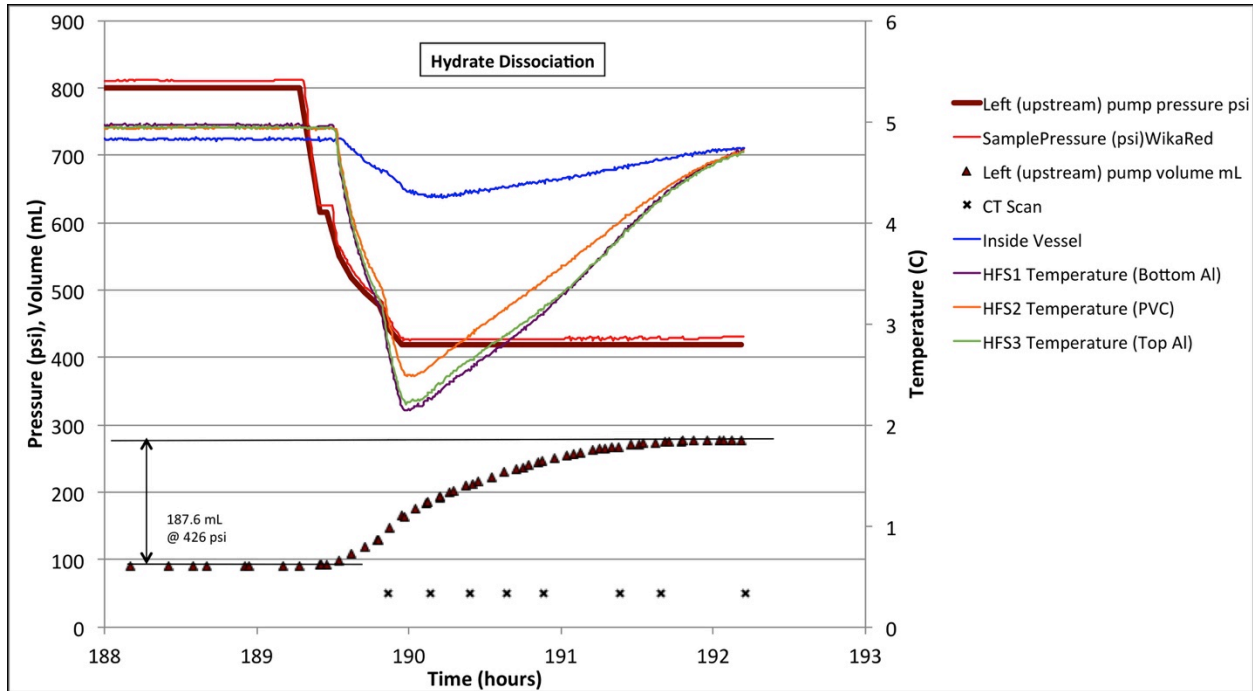


Figure 7. Pressure, temperature, and volume during depressurization.

## Discussion

Capillary pressure is governed by the geometry and wettability of pores and pore throats, and interfacial tension as described by the Young-Laplace equation.

$$P_c = \gamma \left( \frac{1}{R_1} + \frac{1}{R_2} \right) \cos\theta$$

where  $\gamma$  is the interfacial tension,  $\theta$  is the contact angle (indicator of wettability), and the term in parentheses is the Kelvin radius where  $R_1$  and  $R_2$  are orthogonal radii of curvature. Every layered system will have different capillary entry pressures (the pressure required to force a fluid into a material saturated by another fluid) in each layer, and can have a capillary entry pressure gradient for example in a unit fining upwards. Methane hydrate in pores affects the geometry of the pores depending on where it forms, and may alter the wettability. In experiments we have performed to date, both the sand and hydrate have behaved as very water-wetting materials. In this experiment, a gradient in capillary entry pressure was demonstrated in Figure 4, where a nonuniform water saturation was measured in the coarse sand, and this is further contrasted to the sandstone which has smaller pores than the sand, and remained mostly saturated during the drainage. At the end of the drainage, the capillary pressure throughout the sample should have been nearly the same, but affected by gravity.

Hydrate formation began in the coarse larger pores. The concentration of methane in the water in the tight sandstone layer would be governed by diffusion resulting in a gradient that would favor hydrate formation on the outside of that layer. Where hydrate forms, it consumes liquid water resulting in solid material in the pores, reducing the effective pore size. This reduction causes water to flow towards hydrate formation from somewhere else. Our observations in this experiment are that hydrate formation caused local capillary pressure gradients that induced water to flow towards the hydrate from both the coarse sand layer, and also from the tighter sandstone. Thus the partially hydrate-filled pores in the coarse sand became smaller than the hydrate-free pores in the sandstone. This drained the sandstone provided the opportunity for hydrate to form there.

Because our system had relatively high permeability, the effect of depressurization was experienced throughout the sample almost instantaneously. Hydrate dissociated throughout the sample, with the longest lasting hydrate being present in the initially highest water saturation regions in the coarse sand. We did not expect hydrate formation to

occur in the sandstone, yet it formed and began dissociation immediately on depressurization. In the initially dryer regions, the hydrate formed on the faces of the sandstone, whereas in the wetter regions, the hydrate formed throughout the sandstone.

Because of the heterogeneity of the hydrate formation, the placement of the HFSs containing thermocouples were not ideal. It is not clear how the different thermal conductivities of the PVC and aluminum “rounds” affected hydrate formation and dissociation. Hydrate formation was strong at the top and bottom where the high thermal conductivity aluminum rounds were, but the PVC “rounds” did not seem to hinder or help either formation or dissociation. The heterogeneity of the initial water saturation was a much stronger driver of system behavior. The effects of small gradients in expected capillary pressure due to heterogeneity and anisotropy in the natural rock or in packing have not been investigated yet, but are likely to affect overall system behavior, as seen in the middle sandstone layer on the left side in Figure 8. There is a structure in the hydrate dissociation locations and this can be compared to the initial porosity and water saturation distributions.

Heat flux sensors used in this test did not provide data adequate to quantify heat transfer in this system. The thermocouple in each functioned as expected, however the HFS did not. The HFS is composed of a number of thermocouples placed on either side of a material of known thermal conductivity. The thermocouples are placed in series to provide a larger signal than a single thermocouple. A number of things could have caused malfunction. The first is water. These devices are manufactured for use while dry. Our system required not only submersion, but submersion under pressure. Although we took reasonable precautions, any leak into the HFS could partially short a portion of the thermocouples, overwhelming the comparison of signals from the two sides.

Layered systems are very important in natural gas hydrate systems and in the production of gas from gas hydrate. This study has shed some light on gas hydrate dissociation in an anisotropic medium with a mild capillary entry pressure differential. Other studies, such as the study by Seol and Kneafsey (2009) provide additional information on layered systems. In both of these studies, the contrast in capillary entry pressure was mild, and the structural integrity of the sample was sufficient (although a hydrate-formation induced fracture was observed in the earlier study). Natural systems containing higher property contrasts including sands and muds are being studied to observe the magnitude of processes of concern, particularly geomechanical and flow processes.

## References

- [1] Collett, T. S., R. E. Lewis, W. J. Winters, M. W. Lee, K. K. Rose and R. M. Boswell (2011). "Downhole well log and core montages from the Mount Elbert Gas Hydrate Stratigraphic Test Well, Alaska North Slope." *Marine and Petroleum Geology* **28**(2): 561-577.
- [2] Colwell, F., R. Matsumoto and D. Reed (2004). "A review of the gas hydrates, geology, and biology of the Nankai Trough." *Chemical Geology* **205**(3-4): 391-404.
- [3] Kneafsey, T. J., H. Lu, W. Winters, R. Boswell, R. Hunter and T. S. Collett (2011). "Examination of core samples from the Mount Elbert Gas Hydrate Stratigraphic Test Well, Alaska North Slope: Effects of retrieval and preservation." *Marine and Petroleum Geology* **28**(2): 381-393.
- [4] Seol, Y. and T. J. Kneafsey (2009). "X-ray computed-tomography observations of water flow through anisotropic methane hydrate-bearing sand." *Journal of Petroleum Science and Engineering* **66**(3-4): 121-132.

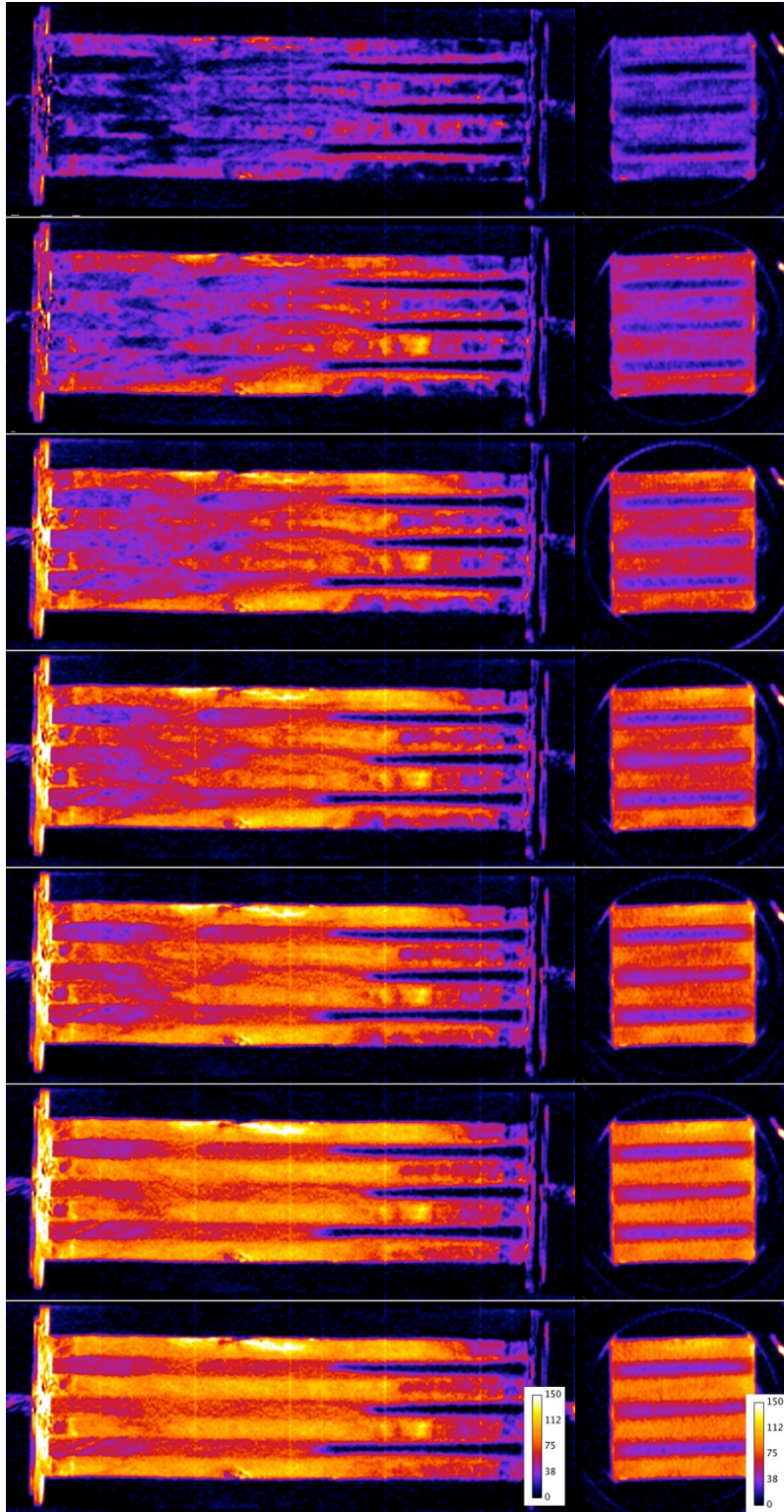


Figure 8. Average differences of the saturated hydrate bearing sediment across the sample (left) and along the sample (right) during depressurization (dissociation) (top is early - 189 hours, bottom late - 192 hours). Black color indicates no decrease in density, and the largest decrease in density (e.g. from water saturated to mostly gas saturated) in yellow/white

## National Energy Technology Laboratory

626 Cochrans Mill Road  
P.O. Box 10940  
Pittsburgh, PA 15236-0940

3610 Collins Ferry Road  
P.O. Box 880  
Morgantown, WV 26507-0880

1450 Queen Avenue SW  
Albany, OR 97321-2198

Arctic Energy Office  
420 L Street, Suite 305  
Anchorage, AK 99501

Visit the NETL website at:  
[www.netl.doe.gov](http://www.netl.doe.gov)

Customer Service Line:  
1-800-553-7681



U.S. DEPARTMENT OF  
**ENERGY**

**NATIONAL ENERGY  
TECHNOLOGY LABORATORY**